TU Delft

Delft University of Technology

Document Version
Final published version

Licence
CC BY

Citation (APA)
Hessels, T., Bastiaanssen, W., Stigter, T., Davids, J., Schoups, G., & Perry, C. (2026). On the determination of pixel-based groundwater withdrawals using SWEO water accounting procedures. Part 1: methodology. *Journal of Water and Climate Change*, *17*(9), 2484-2512. https://doi.org/10.2166/wcc.2026.225

Important note
To cite this publication, please use the final published version (if applicable).
Please check the document version above.

Copyright
In case the licence states “Dutch Copyright Act (Article 25fa)”, this publication was made available Green Open Access via the TU Delft Institutional Repository pursuant to Dutch Copyright Act (Article 25fa, the Taverne amendment). This provision does not affect copyright ownership.
Unless copyright is transferred by contract or statute, it remains with the copyright holder.

Sharing and reuse
Other than for strictly personal use, it is not permitted to download, forward or distribute the text or part of it, without the consent of the author(s) and/or copyright holder(s), unless the work is under an open content license such as Creative Commons.

Takedown policy
Please contact us and provide details if you believe this document breaches copyrights.
We will remove access to the work immediately and investigate your claim.

This work is downloaded from Delft University of Technology.

Journal of
Water & Climate Change

Check for updates

IWA PUBLISHING

© 2026 The Authors

Journal of Water and Climate Change Vol 17 No 9, 2484 doi: 10.2166/wcc.2026.225

On the determination of pixel-based groundwater withdrawals using SWEO water accounting procedures. Part 1: methodology

Tim Hessels [a,*], Wim Bastiaanssen [a,b], Tibor Stigter [c], Jeffrey Davids [d,e], Gerrit Schoups [a] and Chris Perry [f]

[a] Department of Water Management, Faculty of Civil Engineering and Geosciences, Delft University of Technology, Delft, The Netherlands
[b] Hydrosat, Wageningen, The Netherlands
[c] Department of Water Resources and Ecosystems, IHE Delft Institute for Water Education, Delft, The Netherlands
[d] California State University, Chico, CA, USA
[e] Davids Engineering, Chico, CA, USA
[f] Independent consultant, London, UK
*Corresponding author. E-mail: T.M.Hessels@tudelft.nl; timhessels@hotmail.com

TH, 0000-0002-7264-7220; WB, 0000-0002-7931-5018; TS, 0000-0003-4096-2055; JD, 0000-0003-4343-5410; GS, 0000-0002-2552-7293; CP, 0000-0002-9003-7477

ABSTRACT

Groundwater is a critical resource for human and ecosystem needs, yet its availability is increasingly stressed by over-abstractions as well as climate change. Monitoring remains challenging due to limited data of well abstractions, regular piezometric readings, and complex subsurface processes. This study presents Scalable Water balance from Earth Observations (SWEO), a novel water accounting framework that estimates groundwater recharge and withdrawals without requiring detailed hydrogeological information, complex groundwater flow models, hydraulic heads, or metered abstractions. The framework is mainly driven by satellite-based remote sensing data of rainfall surplus/deficit and storage changes into spatially distributed key groundwater balance terms by sequentially applying long- and short-term water balances at local and basin scales. River discharge measurements are used to internally calibrate percolation and baseflow. The framework is transparent, scalable, and applicable to large basins with groundwater irrigation. SWEO can be implemented in the cloud, and processing 25 years can be completed within a few days. The groundwater resource information generated by SWEO is currently not available to groundwater policymakers for preparing longer term policies to make aquifer abstractions more sustainable. An accompanying article describes the validation of this new analytical framework for surface water and groundwater accounting.

Key words: groundwater recharge, groundwater withdrawals, hydrology, scalable water balance, SWEO, water accounting

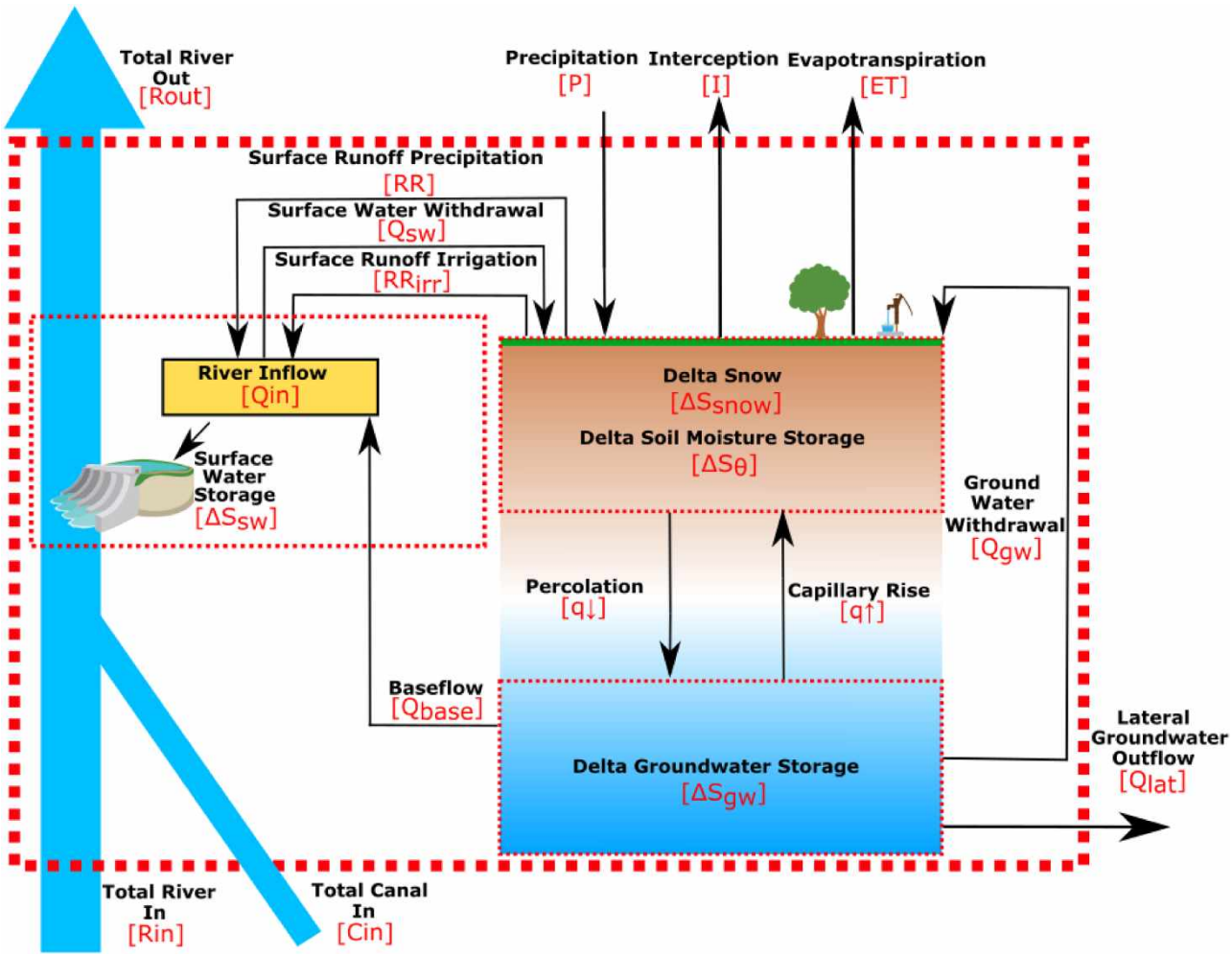
HIGHLIGHTS

- Scalable Water balance from Earth Observations: a novel transparent, scalable, remote sensing-based framework for water accounting.
- Closes the water balance at pixel and basin scales.
- Estimates groundwater recharge and withdrawals without detailed hydrogeology.
- Enables groundwater assessment in large and data-scarce regions.

This is an Open Access article distributed under the terms of the Creative Commons Attribution Licence (CC BY 4.0), which permits copying, adaptation and redistribution, provided the original work is properly cited (http://creativecommons.org/licenses/by/4.0/).

Downloaded from iwaponline.com/jwcc/article-pdf/17/9/2484/1638061/jwc2026225.pdf
by Delft University of Technology user

GRAPHICAL ABSTRACT



1. INTRODUCTION

Groundwater is a critical element in the hydrological cycle, providing both temporary and long-term storage of water that can be accessed in the absence of rainfall or access to surface water. As such it is an essential and reliable source of water for drinking, industries, irrigated agriculture, and natural environments including groundwater dependent ecosystems (GDEs). GDEs are natural habitats or ecological communities that rely on water stored beneath the Earth's surface for its survival (Rohde *et al.* 2024). These ecosystems such as forest and savannahs require groundwater discharge or access to the shallow or deep water table. Seepage zones in mountainous terrain also have a permanent inflow of groundwater that they consume. Population growth and economic development have increased the demand for groundwater in particular (Oki & Kanae 2006; Sharaf 2011; Niazi *et al.* 2024). Irrigated agriculture is the dominant consumptive user of groundwater. Global hydrological models such as WaterGAP estimate that approximately 545 km^3 $year^{-1}$ of groundwater is consumed for irrigation, representing about 43% of total irrigation water consumption, so that some 40% of food production depends on groundwater (Biemans 2012; Wada *et al.* 2014). Critically, only about 50% of the groundwater supplied for irrigation is renewable, in the sense that annual recharge replenishes abstraction. Wada *et al.* (2010) estimated that global groundwater depletion in sub-humid to arid regions was 283 (±40) km^3 $year^{-1}$ in 2000, having doubled in the previous 40 years. This is an entirely unsustainable scenario reflected by declining groundwater levels in many aquifers. Opportunities for enhanced recharge are limited (Stigter *et al.* 2023).

Downloaded from iwaponline.com/jwcc/article-pdf/17/9/2484/1638061/jwc2026225.pdf
by Delft University of Technology user

A recent UN report introduces the concept of 'water bankruptcy' (Madani 2026) arguing that many aquifers (and river basins) have entered a post-crisis condition, in which historical baselines are no longer attainable without transformative change. Financial bankruptcy, the situation where current assets are inadequate to meet current obligations, requires radical restructuring of available assets. Water bankruptcy similarly requires both a more accurate assessment of the over-commitment of renewable groundwater resources, and political decisions involving all stakeholders to agree the priorities for redistributing water resources at sustainable levels. This will involve the definition and enforcement of legal upper bounds to withdrawals at substantially reduced levels. The unattractive alternative is chaotic and unmanaged reductions in supply as aquifers and river systems collapse (Perry 2019), a scenario that is already evident in some severely stressed areas or being hidden by ongoing depletion of aquifers that took centuries or millennia to accumulate.

These trends highlight the urgent need for effective groundwater allocation policies. The California Sustainable Groundwater Management Act (Lubell *et al.* 2020) is one such example, but any such plan requires credible data on the resource, its current distribution, likely future status, and the impact that potential interventions would have.

Several initiatives have attempted to improve groundwater information through databases and hydrological modelling. The International Groundwater Resources Assessment Centre (IGRAC) compiled an open-access database containing global groundwater information, including groundwater abstractions; the World-wide Hydrogeological Mapping and Assessment Program (WHYMAP) provides datasets on aquifers, groundwater recharge, vulnerability to floods and droughts, and transboundary aquifer systems. Wada *et al.* (2010) and Huang *et al.* (2018) downscaled national groundwater statistics to gridded datasets, while Siebert *et al.* (2010) developed a global inventory of areas irrigated with groundwater. Despite these advances, local information on groundwater conditions remains unreliable and scarce.

Modelling studies have been conducted to estimate groundwater withdrawals and storage changes. However, groundwater flow is a complex, nonlinear process involving strongly heterogeneous geological formations and soil characteristics. Groundwater systems are also hydrologically connected to processes in the unsaturated zone (Le Maitre *et al.* 1999; Bastiaanssen *et al.* 2007) and interact with surface water systems (Kalbus *et al.* 2006). Approaches that depend on detailed hydrogeological information or complex groundwater flow models are difficult to apply at large spatial scales due to limited data availability and uncertainties in geological parameters.

Local groundwater assessments are constrained by limited monitoring data and complex subsurface modelling requirements, restricting their applicability for large-scale and data-scarce regions. In particular, withdrawals from private wells and small-scale irrigation systems are frequently unmetered or not publicly reported. Furthermore, GDEs and conjunctive use of surface water and groundwater are often poorly represented in existing databases and models. As a result, significant uncertainties remain regarding the spatial distribution of groundwater recharge and abstraction.

Appropriate groundwater policies and interventions cannot be prepared without inclusion of these interactions. Consequently, monitoring groundwater conditions and quantifying groundwater fluxes at large spatial scales are essentially unresolved. Global scale groundwater flow models are not going to solve this problem, and there is a need for new tools. Knowledge on total renewable water resources and allocation across different water use sectors needs to be improved and be made available to decision makers. The benefits/services of groundwater consumed and level of groundwater over-draft should be evaluated in a simple to understand format, and the tool presented in this article aims to fill this data void.

The development of global remote sensing datasets offers opportunities to address these data gaps. This study presents a Scalable Water balance from Earth Observations (SWEO), which integrates various remotely sensed data sources.

Satellite missions such as the Gravity Recovery and Climate Experiment (GRACE) provide estimates of changes in terrestrial water storage, including groundwater storage (Tapley *et al.* 2004; Lee *et al.* 2011). GRACE has a relatively coarse spatial resolution and does not directly provide information on groundwater fluxes such as recharge or withdrawals. Recent developments in satellite-based hydrological products now provide globally consistent estimates of precipitation (P), actual evapotranspiration (ET), and soil moisture. These datasets enable the analysis of rainfall surplus or deficit (P-ET), which can provide valuable insights into groundwater recharge (P > ET) and groundwater use (ET > P). An additional advantage of using remotely sensed ET data is that ET is enhanced by irrigation withdrawals, floods, wetlands, shallow water tables, capillary rise, groundwater pumping, and natural withdrawals by GDE. Several studies have demonstrated the potential of the ET > P approach. For example, Ahmad *et al.* (2005), Cheema *et al.* (2014), and Simons *et al.* (2020) estimated groundwater abstractions for irrigation in the Indus Basin using remotely sensed P-ET data combined with additional hydrological information.

Downloaded from iwaponline.com/jwcc/article-pdf/17/9/2484/1638061/jwc2026225.pdf
by Delft University of Technology user

To systematically quantify water fluxes and storage changes, several frameworks have been developed. One example is the Water Accounting and Auditing (WA&A) framework developed by the Food and Agriculture Organization (FAO), which aims to improve water-related information for water management and policy development (Batchelor *et al.* 2016). Karimi *et al.* (2013) published the Water Accounting Plus methodology using remote sensing data, but the methodology did not contain auto-calibration procedures based on discharge measurements.

This article sets out a new generic water accounting method that focuses on groundwater recharge and withdrawal processes. The approach builds on the SWEO framework (Hessels *et al.* 2022) and utilizes globally available remote sensing products for precipitation, evapotranspiration, and related hydrological variables. By relying exclusively on open-access datasets and avoiding complex hydrogeological parameterization, the method aims to provide a transparent, easily applicable, and scalable framework for groundwater assessment that can support water accounting and policy development across diverse regions.

Validation case studies for the Aconcagua (Chile), Platte (USA), and Madera (USA) basins are presented in a separate paper (Hessels *et al.* 2026).

2. METHODS

2.1. SWEO conceptual framework

The hydrological system consists of multiple interacting water sources, including atmospheric water, soil water, surface water, and groundwater. These components normally have different hydrological characteristics, storage capacities, and response times, which makes their explicit representation challenging, particularly at large spatial scales encompassing composite land uses.

SWEO is a water accounting framework based on earlier works of Molden (1997), Bastiaanssen (2009), Karimi *et al.* (2013), and Hessels *et al.* (2022). It adopts a simplified two-layer conceptual representation of the hydrological system on a monthly basis consisting of two vertically connected layers: root zone soil water balance and an underlying deeper groundwater layer. Atmospheric water inputs enter the system through P, while ET represents the main atmospheric water flux leaving the system. Surface water interactions are represented through river inflows and outflows, canal transfers, runoff, and surface water withdrawals. Groundwater processes are represented through groundwater withdrawals, baseflow contributions to rivers within the basin, lateral groundwater flow contributions from other basins or toward a river within another basin, capillary rise to the root zone, and deep percolation from the root zone to the groundwater layer.

Instead of modelling each hydrological process in detail using complex hydrogeological parameters, the SWEO framework integrates these processes within a set of coupled water balance equations at each model grid cell and (sub)basin scale. In this way, atmospheric, soil water, surface water, and groundwater fluxes are combined through the conservation of mass within the water balance framework. This conceptual simplification allows the framework to represent the combined effects of multiple hydrological processes while maintaining transparency and minimizing the need for detailed geo-hydrological datasets.

The framework integrates multiple spatial and temporal resolutions of various data layers at different stages of the modelling process and calibrates certain coefficients and bias factors for acquiring consistent water balances.

To enhance clarity in the mathematical equations, parameters are assigned temporal superscripts: ‘d’ stands for daily inputs, ‘y’ for yearly inputs, and ‘lt’ for long term that reflects the total time series being modelled. Spatial superscripts are also introduced, where ‘b’ denotes parameters applied to the entire basin and ‘sb’ represents parameters specific to sub-basins. Furthermore, a source superscript is used to indicate the origin of the dataset: ‘org’ refers to original spatial data from satellites or other sources, while ‘meas’ signifies measured data.

The general structure of a parameter PARA follows the format:

$$\mathrm{PARA}^{\mathrm{source,\ spatial,\ temporal}}$$

If a superscript is not specified, the default spatial and temporal resolution is assumed, which corresponds to pixel-based data on a monthly timescale. Pixel size is determined by the modelling grid, which depends on the input data and typically ranges from 100 to 250 m.

Downloaded from iwaponline.com/jwcc/article-pdf/17/9/2484/1638061/jwc2026225.pdf
by Delft University of Technology user

2.2. Water balance equations

The SWEO framework characterizes the overall water balance of a (sub)basin as follows:

$$P^{sb} + R_{in}^{sb} + C_{in}^{sb} = R_{out}^{sb} + I^{sb} + ET^{sb} + \Delta S_{tot}^{sb} + Q_{lat}^{sb} \quad (1)$$

where P is the precipitation (mm month^{-1}), I is the interception (mm month^{-1}), ET is the evapotranspiration (mm month^{-1}), ΔS_{tot} is the total change in water storage (mm month^{-1}), R_{in} is the total river inflow (mm month^{-1}), R_{out} is the total river outflow (mm month^{-1}), C_{in} is the net canal discharge, representing water transferred between basins through aqueducts (mm month^{-1}), and Q_{lat} is the net lateral groundwater outflow, exiting through groundwater layers (mm month^{-1}).

In the overall water balance, the total water storage change (ΔS) is the total water storage of four distinct components: (i) ΔS_θ, representing changes in soil moisture storage within the root zone; (ii) ΔS_{snow}, defines the water storage change within snow bodies; (iii) ΔS_{gw}, accounting for changes in groundwater storage in the deeper subsurface; and (iv) ΔS_{sw}, which constitutes the water storage change of waterbodies such as rivers, lakes, and reservoirs.

The overall water balance will be divided into the following three distinct sub-water balances: (i) the soil water balance, (ii) the groundwater balance, and (iii) the river water balance.

(i) The soil water balance for a pixel is given by the following equation:

$$P + Q_{sw} + Q_{gw} + q_\uparrow = ET + I + RR + RR_{irr} + q_\downarrow + \Delta S_\theta + \Delta S_{snow} \quad (2)$$

where Q_{sw} is the irrigation provided by surface water withdrawal (mm month^{-1}), Q_{gw} is the irrigation provided by groundwater withdrawal (mm month^{-1}), $q\downarrow$ is the capillary rise from shallow groundwater tables (mm month^{-1}), $q\uparrow$ is the deep percolation below the root zone (mm month^{-1}), RR is the surface runoff generated by precipitation or snowmelt events (mm month^{-1}), RR_{irr} is the surface runoff resulting from irrigation activities (mm month^{-1}), ΔS_θ is the difference in water stored within the soil root zone (mm month^{-1}), and ΔS_{snow} is the difference in volume of water accumulated in the form of snow (mm month^{-1}).

(ii) The groundwater balance can also be determined per pixel and reads as follows:

$$q_\downarrow = Q_{gw} + Q_{base} + Q_{lat} + q_\uparrow + \Delta S_{gw} \quad (3)$$

where Q_{base} is the groundwater baseflow, which contributes to river discharge (mm month^{-1}), and ΔS_{gw} is the difference in water stored in the deeper groundwater layer (mm month^{-1}).

(iii) The final water balance of the river is applicable only at the (sub)basin level:

$$R_{in}^{sb} + C_{in}^{sb} + RR^{sb} + RR_{irr}^{sb} + Q_{base}^{sb} = R_{out}^{sb} + Q_{sw}^{sb} + \Delta S_{sw}^{sb} \quad (4)$$

where ΔS_{sw} is the difference in volume of water stored in lakes and reservoirs (mm month^{-1}).

Figure 1 provides a comprehensive overview of different water balances, encompassing all the hydrological fluxes and states as described by the previous water balance equations.

2.3. Required input data

The minimal required inputs can be acquired from independent open-access satellite data archives, as outlined in Table 1. Further details regarding the necessary SWEO inputs are elaborated by Hessels *et al.* (2022).

Each data source contains inherent uncertainties, and directly combining these products may lead to unrealistic or internally inconsistent water balance estimates. A substantial part of this uncertainty can be addressed through validation of the input data prior to their use in modelling applications. For example, local measurements can be used to constrain and validate water balance components, as demonstrated by Mourad *et al.* (2024a, b), who performed a prior uncertainty analysis providing baseline uncertainty estimates for key variables that can be further reduced through the integration of additional (local) observations. In addition, cross-validation approaches can be used to assess the consistency among different data

Downloaded from iwaponline.com/jwcc/article-pdf/17/9/2484/1638061/jwc2026225.pdf
by Delft University of Technology user

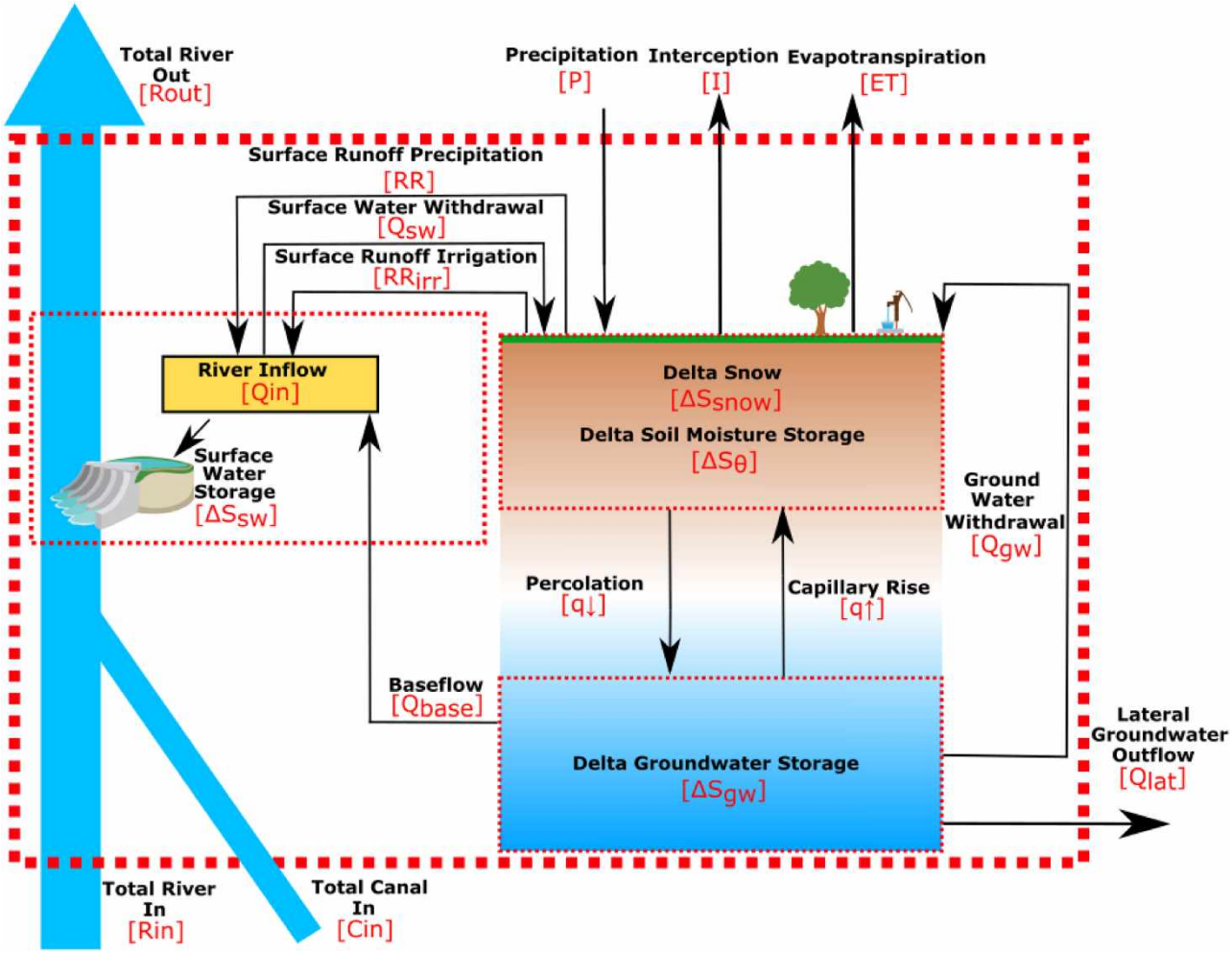


Figure 1 | Schematic view of flows and fluxes at the pixel and river basin scale. Various terms are determined from remote sensing measurements and are plugged into the framework.

products. Such methods may include probabilistic bias correction and noise filtering to improve the consistency of estimated water balance fluxes and state variables across datasets (Schoups & Nasseri 2021; Mourad *et al.* 2026).

Beyond these pre-processing steps, the SWEO framework itself employs a strict internal calibration sequence that leverages the strengths of each data type to cross-validate other sources using mass balances. This is achieved by analysing the overall water balance or its subcomponents, while also considering variations in temporal and spatial resolution. In this way, inconsistencies between different satellite products can be identified and reduced during the modelling process.

2.4. Model workflow

The complete SWEO methodology consists of ten sequential steps. These steps are schematically illustrated in the flowchart presented in Figure 2 and are described in detail in the following sections.

2.4.1. Step 1: calculate the long-term water balance for the (sub)basin to bias-correct monthly ET

The initial step in the SWEO process involves calibrating the water balances across the entire river basin to perform a long-term calibration for ET. Long-term here refers to the entire modelling period, which should ideally cover 20 years or longer. The longer the period, the smaller the relative contribution of total water storage changes (ΔS_{tot}), thereby minimizing their impact on the accuracy of the overall water balance. By applying the bulk water balance to the entire drainage area, internal water displacements can be neglected. This means that local vertical and horizontal movements within the basin become

Downloaded from iwaponline.com/jwcc/article-pdf/17/9/2484/1638061/jwc2026225.pdf
by Delft University of Technology user

Table 1 | Overview of the minimum required input data for the SWEO model, along with example data sources

Variable	Temporal resolution	Source example
Precipitation	Daily	CHIRPS, TRMM, GPM, PERSIANN, TMPA, IMERG, CMORPH, GSMaP
ET actual	Monthly	WaPOR, SEBAL, OpenET, SSEBop, ALEXI, GLEAM, CMRSET, SEBS, MODIS (MOD16)
ET_0 reference	Monthly	FEWS, MERRA, WaPOR
Air temperature	Monthly	GLDAS, MERRA, GEOS
Leaf area index	Monthly	MODIS (MOD15), Sentinel-3/OLCI (LAI)
fPAR	Monthly	MODIS (MOD15), Sentinel-3/OLCI (FAPAR)
Snow cover	Monthly	MODIS (MOD10), Sentinel (CLMS)
Groundwater Storage	Monthly	GRACE
Water body area	Monthly	JRC
Altitude and drainage direction	–	HydroShed, SRTM, ASTERdem
Land cover	–	GlobCover, MODIS (MCD12)
Soil properties	–	SoilGrids
Piezometric heads and fluctuation	–	PCR-GLOBWB

irrelevant. Accordingly, the water balance for the basin is expressed as follows:

$$P^{b,lt} + R_{\text{in}}^{b,lt} + C_{\text{in}}^{b,lt} = R_{\text{out}}^{b,lt} + I^{b,lt} + ET^{b,lt} + \Delta S_{\text{tot}}^{\text{GRACE},b,lt} + Q_{\text{lat}}^{\text{org},b,lt} \quad (5)$$

Change in water storage: The ΔS_{tot} includes the total change of surface water (ΔS_{sw}), unsaturated zone (ΔS_{θ}), snow (ΔS_{snow}), and groundwater (ΔS_{gw}). A valuable remote sensing product for assessing this ΔS_{tot} is GRACE that provides water equivalent height (WEH) measurements representing the change in water column height relative to the initial state. By calculating the difference in WEH value over a given period, the $\Delta S_{\text{tot}}^{\text{GRACE}}$ is quantified over that period. The downside of GRACE is the coarse spatial resolution of 250 km. This limits the effectiveness of usage at local or small watershed scales (Vishwakarma *et al.* 2018).

Precipitation: Except for hyper-arid climates, precipitation (P) constitutes the primary source of water for the basin. Multiple remote sensing-based P products are available and have been previously evaluated for their performance under various climatic conditions (e.g., Hessels 2015; Dembélé & Zwart 2016; Dinku *et al.* 2018; Zeng *et al.* 2018; Camberlin *et al.* 2019). Depending on the climatic conditions of the basin, the most suitable remote sensing-based P product can be selected. Prior to the application in SWEO, P inputs may be further improved through bias correction using local rain gauge observations or applying cross-validation approaches. The SWEO model directly uses the precipitation data provided by the user.

Interception: Interception (I) is the process by which P is captured by vegetation, buildings, or other surfaces before it reaches the soil surface. Interception can be explicitly defined as model input. If not provided, SWEO estimates interception based on vegetation cover (VC) and the leaf area index (LAI). The VC can either be specified directly or, if not provided, SWEO derives the VC from the LAI using the following formula (Kustas & Anderson 2009):

$$\text{VC} = 1 - \text{EXP}(-0.5 \times \text{LAI}) \quad (6)$$

The interception is determined using the formulation presented by von Hoyningen-Hüne (1983) and Braden (1985):

$$I = I_{\max} \times \text{LAI} \times \left(1 - \frac{1}{1 + \left(\frac{P}{\text{RD}} \times \text{VC}\right)/(I_{\max} \times \text{LAI})}\right) \times \text{RD} \quad (7)$$

Downloaded from iwaponline.com/jwcc/article-pdf/17/9/2484/1638061/jwc2026225.pdf
by Delft University of Technology user

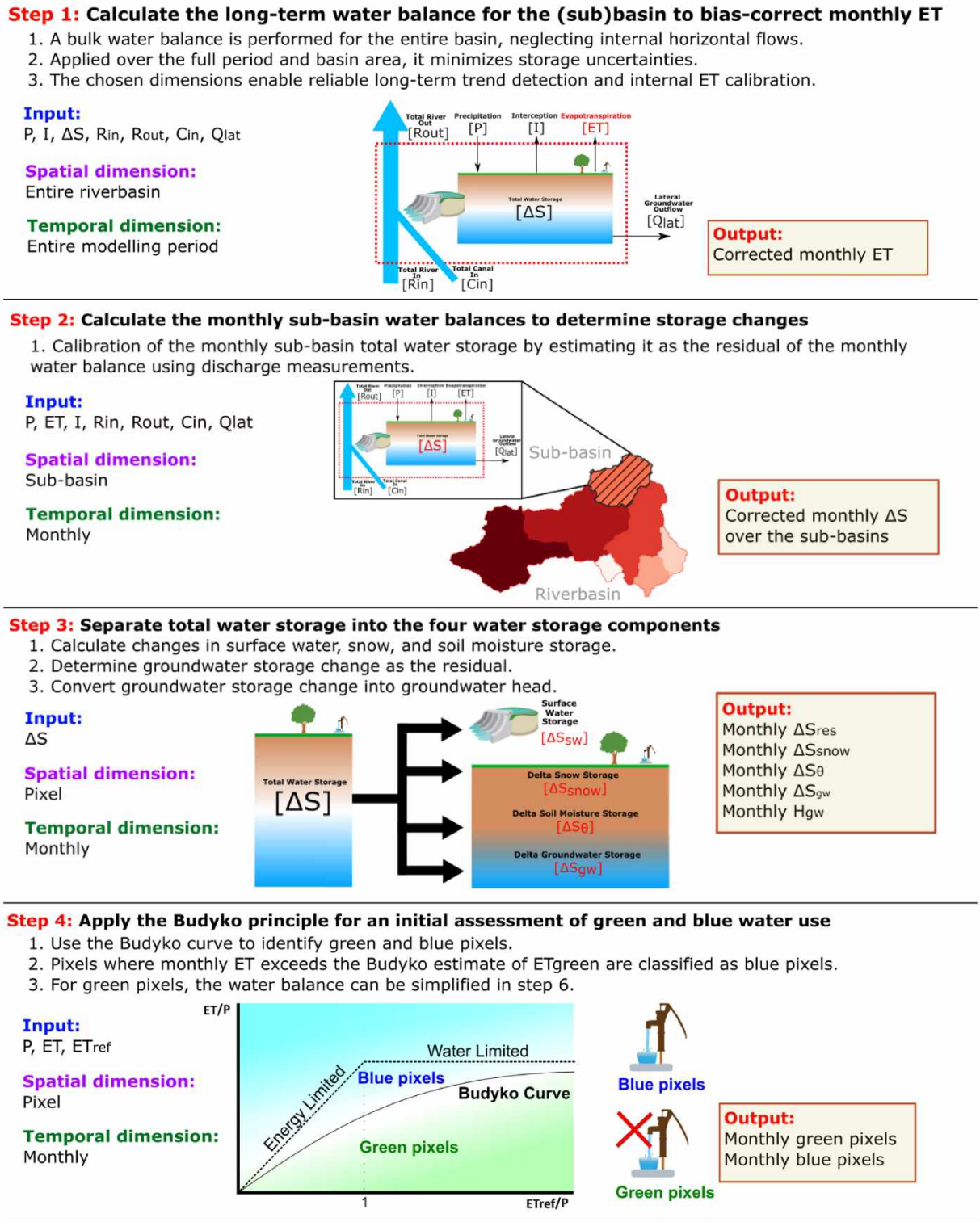


Figure 2 | Schematic flowchart of the ten steps of the SWEO framework. *(continued).*

Downloaded from iwaponline.com/jwcc/article-pdf/17/9/2484/1638061/jwc2026225.pdf
by Delft University of Technology user

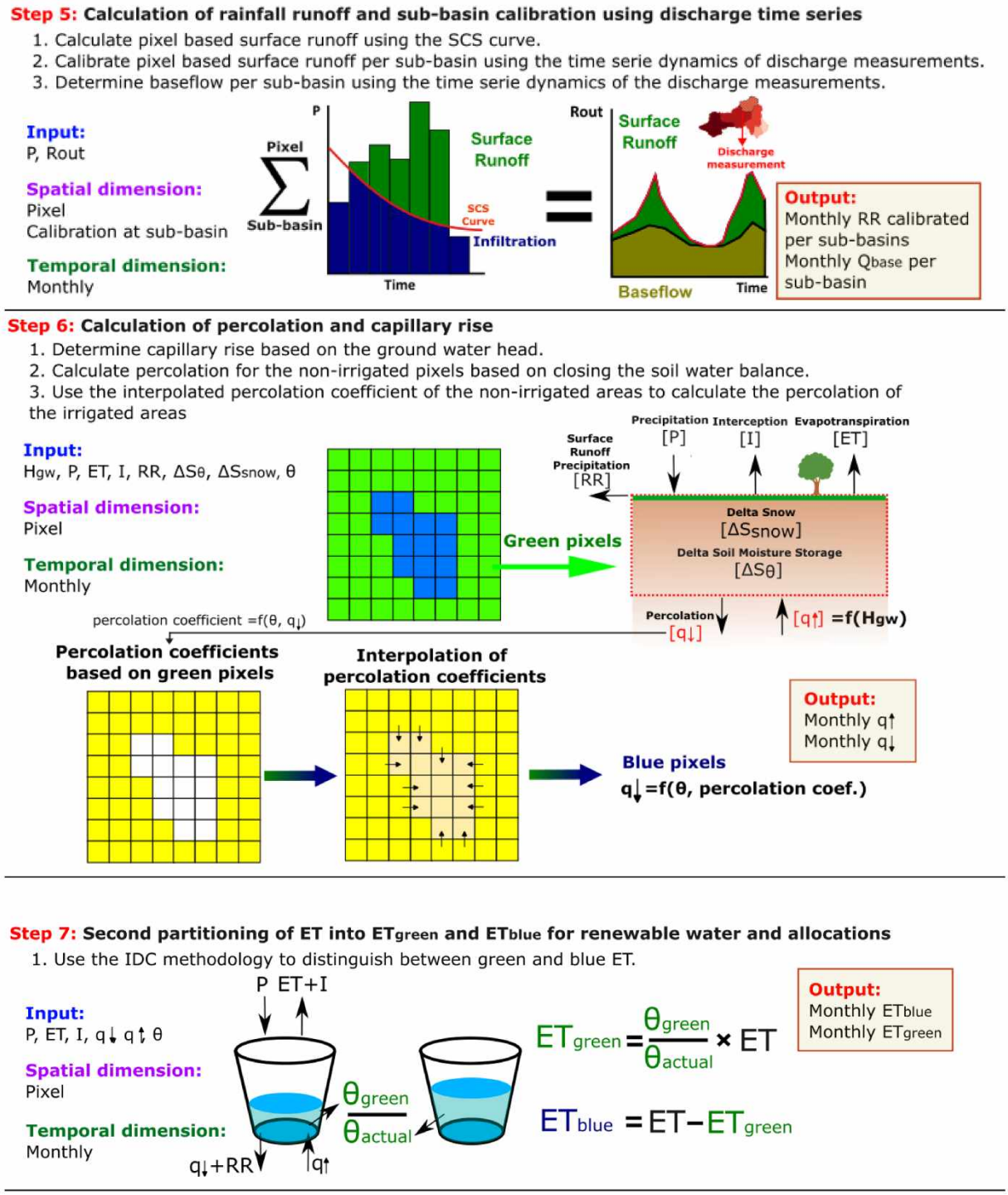


Figure 2 | Continued.

Downloaded from iwaponline.com/jwcc/article-pdf/17/9/2484/1638061/jwc2026225.pdf
by Delft University of Technology user

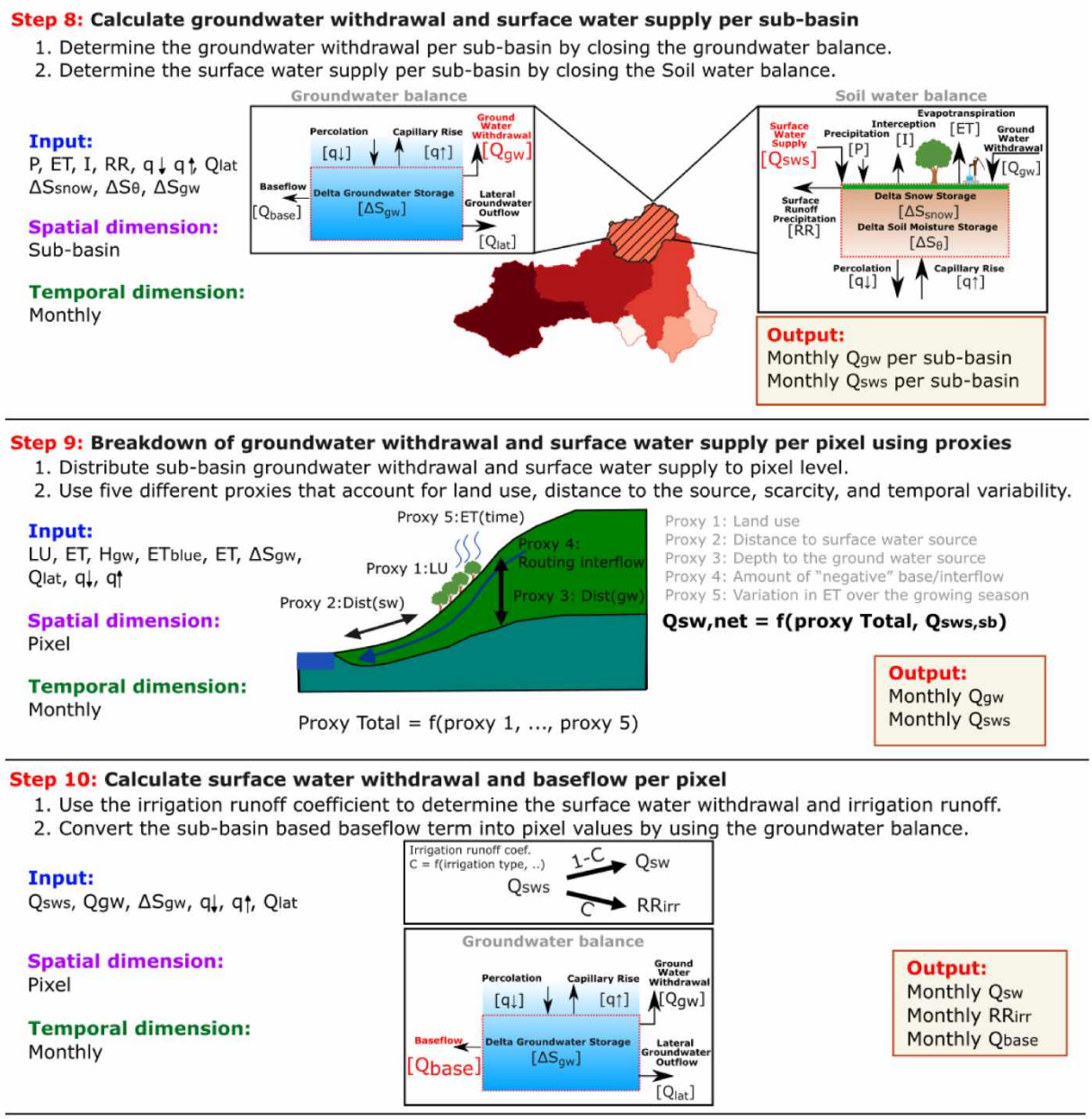


Figure 2 | Continued.

where VC is the vegetation cover fraction (–); LAI is the leaf area index (m^2 m^{-2}); I_{max} is the maximum interception per leaf (mm day^{-1}), set to a default value of 0.6 mm day^{-1}; and RD is the number of rainy days (day $month^{-1}$), defined as the count of days when daily precipitation exceeds 0.5 mm day^{-1}.

Lateral groundwater flow: The lateral outflow ($Q_{lat}^{org,\,b}$)represents net lateral groundwater flow of the deepest model layer into or out of the basin. This component of groundwater flow occurs laterally toward adjacent river basins, rather than discharging into the basin's own river system.

Since lateral groundwater flow is not constrained by surface topography, a (sub)basin may also receive a net influx of lateral groundwater from surrounding areas. Consequently, $Q_{lat}^{org,b}$ can take positive values (net outflow) or negative values (net inflow).

Downloaded from iwaponline.com/jwcc/article-pdf/17/9/2484/1638061/jwc2026225.pdf
by Delft University of Technology user

In many case studies, terms related to net lateral inflow can be neglected. This simplification is justified because the water balance is mainly applied to relatively large river basins, where the contribution of net lateral inflow and related terms is small compared with the other dominant hydrological components. As such, it has only a minor effect on the overall water balance.

The total amount of long-term lateral groundwater flow leaving the entire basin can be specified in the model. If this information is not provided, it is estimated using Darcy's equation based on the initial groundwater head distribution.

$$Q_{\text{lat}}^{\text{org},b} = -k_{\text{hor}} \times D \times \frac{\text{GWH}_{\text{outer}} - \text{GWH}_{\text{inner}}}{L^2} \tag{8}$$

where Q_{lat} is the lateral groundwater flow (mm month^{-1}), k_{hor} is the horizontal hydraulic conductivity (mm month^{-1}), D is the thickness of the saturated soil layer and is required as an input parameter (m), $\text{GWH}_{\text{inner}}$ is the groundwater head at the basin boundary (m), $\text{GWH}_{\text{outer}}$ is the groundwater head of the neighbouring pixels located outside the basin (m), L is the distance between pixels, determined by the model resolution (m).

In many areas, k_{hor} and D of a basin are difficult to define accurately. Furthermore, the flow dynamics in hard rock environments are not adequately represented by this equation. Consequently, it is recommended to prescribe a certain total long-term lateral groundwater flow to the model using external sources such as being available from PCRaster Global Water Balance (PCR-GLOBWB) (De Graaf *et al.* 2014a, b). This input can be provided either as (1) spatially distributed data derived from a global groundwater model or (2) as a single aggregated lateral groundwater flow value representing the entire basin. In the latter case, the model applies a spatial distribution approach wherein the total lateral groundwater flow is preserved, and its allocation across sub-basins ($Q_{\text{lat}}^{\text{org,sb}}$) is based on the relative distribution of the groundwater heads. This ensures that the distribution of groundwater flow along the basin boundary reflects the spatial variability in hydraulic gradients and aquifer properties while maintaining the total lateral groundwater flow that is provided by the user.

Discharge: The long-term river outflow from basins, denoted as $R_{\text{out}}^{b,lt}$, is based on flow measurements. Hydro-meteorological posts measure the long-term average discharge. In cases of closed basins, the outflow is negligibly small.

If the entire upstream catchment area of the basin is delineated, the term $R_{\text{in}}^{b,lt}$ can be assumed to be zero, as no upstream river discharge is expected to enter the basin. Similarly, for basins unaffected by anthropogenic activities, the inflow from aqueducts ($C_{\text{in}}^{b,lt}$) can also be neglected. However, in cases where canals or aqueducts facilitate inter-basin transfers, these flows must be explicitly measured or estimated to accurately quantify the net inflow and outflow to the modelled basin.

Evapotranspiration: ET is a key component of the hydrological cycle, representing the combined amount of evaporation from soil, vegetation, and open water surfaces to the atmosphere. Various energy balance methods for ET exist, and each ET algorithm has its own uncertainties. This is also reflected in the range of evapotranspiration values reported by the various ET products, as validated in the previous ET studies (Vinukollu *et al.* 2011; Hofste 2014; Trambauer *et al.* 2014; Knipper *et al.* 2024). Often ET algorithms are calibrated against flux towers with a minor footprint that do not represent the basin's ET. Sriwongsitanon *et al.* (2020) therefore validated basin-scale ET on the basis of measurements of rainfall and river outflow in combination with estimates of storage changes.

The same approach is applied to the ET product used as input to SWEO (ET^{org}), where the resulting bias correction ensures a consistent and closed water balance for the defined hydrological system.

A single bias factor for ET^{org} is computed based on the entire basin and over the full modelling period. This choice of temporal and spatial resolution minimizes errors associated with changes in total water storage of GRACE ($\Delta S_{\text{tot}}^{\text{GRACE},b,lt}$), which are primarily derived from large-scale (250 km by 250 km) GRACE mascons (Loomis *et al.* 2021). Long-term ΔS_{tot} generally represents a relatively minor component of the overall water balance, as it represents a state, rather than a flux. Consequently, despite some uncertainties in $\Delta S_{\text{total}}^{\text{grace}}$, its contribution is small compared with other fluxes, and the impact on the total water balance is limited.

The $\text{ET}^{b,\text{lt}}$ to close the overall long-term water balance of the basin can be estimated by rewriting the overall water balance:

$$\text{ET}^{b,\text{lt}} = P^{b,\text{lt}} + R_{\text{in}}^{b,\text{lt}} + C_{\text{in}}^{b,\text{lt}} - I^{b,\text{lt}} - R_{\text{out}}^{b,\text{lt}} - Q_{\text{lat}}^{\text{org},b,\text{lt}} - \Delta S_{\text{tot}}^{\text{GRACE},b,\text{lt}} \tag{9}$$

By comparing the long-term original evapotranspiration ($\text{ET}^{\text{org,b,lt}}$) with the basin-estimated evapotranspiration ($\text{ET}^{\text{b,lt}}$) from Equation (9), a long-term bias correction factor is derived. This factor is uniformly applied to all $\text{ET}^{\text{org,b}}$ values, ensuring

Downloaded from iwaponline.com/jwcc/article-pdf/17/9/2484/1638061/jwc2026225.pdf
by Delft University of Technology user

consistency with $ET^{b,lt}$. It is assumed that $ET^{org,b}$ accurately captures the spatial distribution of ET, but that the absolute ET values require minor adjustment. The same assumption applies to the temporal disaggregation of annual ET into monthly time steps.

After this first step, P, I, ET, Q_{riv}, and ΔS components are congruent for the overall long-term water balance. In the subsequent steps within the SWEO approach, these fluxes and state will be broken down into local pixel values and monthly timescale.

2.4.2. Step 2: calculate the monthly sub-basin water balances to determine storage changes

The second step aims to enhance the spatial and temporal resolution of ΔS^{sb}_{total}. This enhancement is applied to all sub-basins with available monthly discharge measurements. The drainage areas corresponding to the measurements locations are created from the drainage direction map using a digital elevation model (DEM). For those areas, ΔS_{tot} is calculated as follows:

$$\Delta S^{closed,sb}_{tot} = P^{sb} + R^{meas,sb}_{in} - R^{meas,sb}_{out} + C^{meas,sb}_{in} - I^{sb} - ET^{sb} - Q^{org,\,sb}_{lat} \quad (10)$$

where $\Delta S^{closed,sb}_{tot}$ is the monthly total change in water storage for a sub-basin, derived from the water balance closure (mm month^{-1}), $R^{meas,sb}_{in}$ is the measured monthly river discharge entering the sub-basin (mm month^{-1}), $R^{meas,sb}_{out}$ is the measured monthly river discharge at the outlet of the sub-basin (mm month^{-1}), and $C^{meas,sb}_{in}$ is the measured anthropogenic (canal or managed) flow within the sub-basin (mm month^{-1}).

By moving from upstream to downstream drainage basins, it becomes feasible to apply a cascade-based estimation of $R^{meas,sb}_{out}$ with the most upstream area having zero $R^{meas,sb}_{in}$. The outflow from the most upstream drainage area can then be used as an input for the inflow of the downstream drainage area. Hence, Step 2 should be repeated for all the discharge measurement stations. The monthly ΔS^{sb}_{tot} values thus obtained replaces the $\Delta S^{GRACE,b,lt}_{tot}$, which are less applicable for sub-basins smaller than 62.500 km^2 due to their coarse spatial resolution. The consequence is a proper estimation of monthly storage changes that will have a rather different magnitude due to locally prevailing hydrological processes. Basically, GRACE data are overruled.

2.4.3. Step 3: separate total water storage into the four water storage components

The ΔS_{tot} can be further partitioned into the four distinct water storage components:

$$\Delta S_{tot} = \Delta\, S_{gw} + \Delta\, S_{\theta} + \Delta S_{snow} + \Delta S_{sw} \quad (11)$$

Surface water component: Surface water storage (ΔS_{sw}) plays a key role in transferring water resources from wet to dry seasons. Traditional methods of estimating these storage changes often rely on *in situ* measurements or hydro-dynamic modelling approaches. However, with the use of satellite imagery, it is also possible to monitor and quantify the surface area of lakes and reservoirs over time, providing valuable data for routing reservoir storage. This method has been described in several studies (Duan & Bastiaanssen 2013; Donchyts *et al.* 2017; Condeça *et al.* 2022; Hou *et al.* 2022).

SWEO establishes a quantitative relationship between open water surface area (A_{water}) and water volume (V_{water}) using water level from a DEM. First, water occurrence data from the European Commission's Joint Research Centre (JRC) are used to identify lakes and reservoirs. Next, monthly variations in A_{water}, derived from the JRC monthly water masks, are correlated with changes in water level (L_{water}). Because altimetric water levels are not easily available for all lakes and reservoirs, L_{water} is estimated from the slope and elevation of the surrounding terrain along the water boundary. For each water body, the resulting $L_{water} = f(A_{water})$ relationship is integrated to derive water volumes (V_{water}) and its changes (ΔV_{water}). An analytical relationship between water storage volume and surface area (i.e., $V_{water} = f(A_{water})$) is established for each lake or reservoir using high resolution 30 m monthly A_{water} data. Based on this relation, monthly surface water storage changes (ΔS_{sw}) are determined and used for breaking down the total water storage required for the water balance.

Snow storage component: Water can also be seasonally redistributed through snow storage (ΔS_{snow}). The 8-daily snow cover mask is utilized from Moderate Resolution Imaging Spectroradiometer (MODIS) measurements to identify pixels with snow storage. Time series of snow cover greatly provides insights in the duration of accumulation and melting of snow that impacts river flow. The absolute amount of snowfall (S_f) is determined based on the precipitation rate of pixels classified as snow covered. It is assumed that all precipitation falling on these snow-defined pixels occurs as snowfall.

Downloaded from iwaponline.com/jwcc/article-pdf/17/9/2484/1638061/jwc2026225.pdf
by Delft University of Technology user

The snowmelt (S_m) process is modelled according to the formulation provided by the Soil and Water Assessment Tool (SWAT) model (Neitsch *et al.* 2009). In this approach, S_m is driven by the difference between the average snowpack temperature and the maximum air temperature ($T_{\text{air}}^{\text{max}}$), with snowmelt occurring when temperatures exceed a specified threshold (T_{mlt}):

$$S_m = \max\left(b_{\text{mlt}} \times \left(\left(\frac{T_{\text{snow}} + T_{\text{air}}^{\text{max}}}{2}\right) - T_{\text{mlt}}\right),\ 0\right) \times \text{NOD} \tag{12}$$

where b_{mlt} is the melt factor (mm °C^{-1} day^{-1}), T_{snow} is the temperature of the snowpack (°C), $T_{\text{air}}^{\text{max}}$ is the maximum air temperature (°C), T_{mlt} is the threshold temperature above which snowmelt occurs (°C), NOD is the number of days in the month (days month^{-1}), and T_{snow} from Equation (12) is estimated using the following equation:

$$T_{\text{snow}} = (1 - \text{TIMP}) \times T_{\text{snow}}^{t-1} + \text{TIMP} \times T_{\text{air}}^{t} \tag{13}$$

where TIMP is the snow temperature lag factor (–).

Although SWEO is capable of applying this formulation at a daily time step using hourly meteorological data, a monthly time step is adopted to reduce the volume of input data required for model operation. For this monthly time step, the model estimates the maximum air temperature by adding 3 °C to the monthly mean air temperature. Additionally, the default value for the temperature lag factor (TIMP) is set to 0.95.

For pixels without year-round snow cover, the snowmelt parameter is internally calibrated, ensuring that the seasonally accumulated snowmelt equals the total seasonal snowfall. Accordingly, monthly snowmelt fractions S_f are derived by dividing the calculated monthly snowmelt by the total snowmelt over the entire snow season. These fractions are then applied to the accumulated snowfall within the corresponding months to obtain the adjusted monthly snowmelt for each pixel.

Finally, ΔS_{snow} can be calculated by:

$$\Delta S_{\text{snow}} = S_f - S_m \tag{14}$$

Subsurface water storage component: The change in root zone water storage is determined by the variations in subsurface soil moisture content. Soil moisture content can either be provided as an input from open-access data sources (Hain *et al.* 2011; Mohanty *et al.* 2017; Mourad *et al.* 2024a, b) or estimated from surface energy balance partitioning following the study by Ahmad & Bastiaanssen (2003):

$$\theta_{\text{rel}} = \exp((\Lambda - 1)/0.421) \tag{15}$$

where Λ is the evaporative fraction of the surface energy balance. The value for Λ of 1.0 indicates a fully saturated land that produces negligible sensible heat fluxes. For avoiding net radiation computations, SWEO simplifies the definition of Λ into a relative evapotranspiration factor:

$$\Lambda \approx \frac{\text{ET}}{\text{ET}_{\text{ref}}} \tag{16}$$

In the aforementioned equation, reference evapotranspiration (ET_{ref}) represents the rate of ET from a well-watered reference crop under optimal conditions. Λ is constrained to remain within the range of 0–1. A value of 1.0 indicates that the vegetation is not experiencing any water stress. This condition typically occurs when soil moisture levels are above the field capacity (θ_{FC}) instead of the saturated soil moisture content (θ_{sat}). Therefore, a reduced maximum value of soil moisture in the root zone is considered by taking the average of θ_{sat} and θ_{FC} as the maximum moisture content. Based on this, the volumetric actual soil moisture (θ_{act}) over the total root zone can then be estimated by:

$$\theta_{\text{act}} = \theta_{\text{rel}} \times ((\theta_{\text{sat}} + \theta_{\text{FC}})/2 - \theta_{\text{res}}) + \theta_{\text{res}} \tag{17}$$

where θ_{res} is the residual soil moisture content of the soil. The change in water storage of the top soil can be calculated as

Downloaded from iwaponline.com/jwcc/article-pdf/17/9/2484/1638061/jwc2026225.pdf
by Delft University of Technology user

follows:

$$\Delta S_{\theta}^{t} = (\theta_{\text{act}}^{t} - \theta_{\text{act}}^{t-1}) \times T_{\text{top}} \tag{18}$$

where T_{top} is the thickness of the top layer. By default, T_{top} is considered a constant with a value of 500 mm. However, it can also be treated as a spatially variable parameter dependent on land use. It is a fact that the majority of the moisture changes occur in the upper soil due to infiltration and evapotranspiration.

Groundwater storage component: Because of various groundwater processes being only marginally understood, water stored in the deeper groundwater layer is computed as the residual of all other storage terms. As the total water storage change is validated for each sub-basin in step 2, ΔS_{snow}, ΔS_{θ}, and ΔS_{sw} are first averaged over the sub-basins. These averaged values are then subtracted from $\Delta S_{\text{tot}}^{\text{sb}}$ in each sub-basin. Consequently, the change in bulk groundwater storage (ΔS_{gw}) for a given sub-basin can be defined as follows:

$$\Delta S_{\text{gw}}^{\text{sb}} = \Delta S_{\text{tot}}^{\text{sb}} - \Delta S_{\theta}^{\text{sb}} - \Delta\, S_{\text{snow}}^{\text{sb}} - \Delta S_{\text{sw}}^{\text{sb}} \tag{19}$$

Groundwater storage changes vary spatially due to geological formations and geo-hydrological processes. Historical fluctuations of groundwater levels are used as a proxy to downscale $\Delta S_{\text{gw}}^{\text{sb}}$ to pixel scale. This is achieved using the following equation:

$$\Delta S_{\text{gw}} = \Delta S_{\text{gw}}^{\text{sb}} \times \frac{H_{\text{gw,fluc}}^{\text{lt}} \times S_y}{H_{\text{gw,fluc}}^{\text{sb,lt}} \times S_y^{\text{sb}}} \tag{20}$$

where $H_{\text{gw,fluc}}^{\text{lt}}$ represents the long-term groundwater head fluctuations derived from global groundwater models like PCR-GLOBWB. These heads are converted into groundwater storage change by multiplying by the specific yield (S_y) that varies with geography. Spatial estimates of S_y are determined as a function of the soil clay content of the unsaturated zone (SC_{clay} in percentage) using the following simplified linear equation:

$$S_y = \alpha - \beta \times \text{SC}_{\text{clay}} \tag{21}$$

SWEO uses default parameter values of $\alpha = 0.25$ and $\beta = 0.0038$. The difference in ΔS_{gw} can be re-expressed into a difference in groundwater head (H_{gw} in metres). This provides more consistency in temporal groundwater dynamics:

$$\Delta H_{\text{gw}} = \frac{S_{\text{gw}}}{S_y} \times 0.001 \tag{22}$$

The groundwater heads are essential for getting insights in the lateral movement and capillary rise of water. Using the initial groundwater head from PCR-GLOBWB or a previous SWEO run as starting point, the groundwater head for the modelling period can be determined as follows:

$$H_{\text{gw}}^{t} = H_{\text{gw}}^{t-1} + H_{\text{gw}}^{t} \tag{23}$$

Once all individual water storage changes are determined for each pixel, the pixel-based ΔS_{tot} can be approximated as follows:

$$\Delta S_{\text{tot}} = \Delta\, S_{\text{gw}} + \Delta\, S_{\theta} + \Delta S_{\text{snow}} + \Delta S_{\text{sw}} \tag{24}$$

It is assured that the aggregated value of ΔS_{tot} will yield to$\Delta S_{\text{tot}}^{\text{closed,sb}}$ from Equation (10).

Downloaded from iwaponline.com/jwcc/article-pdf/17/9/2484/1638061/jwc2026225.pdf
by Delft University of Technology user

2.4.4. Step 4: apply the Budyko principle for an initial assessment of green and blue water use

Prior to performing calculations on the soil water balances, each pixel is classified monthly into two categories: pixels receiving rainfall water only (i.e. green water) and pixels that have an extra source of water (i.e., blue water). This first assessment provides step 5 with an initial estimation of water supply from non-rainfall sources and simplifies soil water balance computations in step 6 from pixels that are defined as green water pixels.

The Budyko curve is used to perform this first classification. This curve is a widely recognized conceptual framework used to describe the relationship between long-term mean ET and P in a given basin with certain climatic conditions (Budyko & Miller 1974). The partitioning of available energy and water resources is based on an aridity index.

Numerous studies have described the Budyko curve using empirical formulations (Turc 1954; Budyko & Miller 1974) or analytical derivations (Fu 1981; Zhang *et al.* 2004; Yang *et al.* 2008; Gerrits *et al.* 2009; Simons *et al.* 2020). SWEO employs the empirical formulation as outlined in Budyko's & Miller's original work (1974), expressed as follows:

$$\mathrm{ET}_{\mathrm{act}}^{\mathrm{budyko}}/P = \left(\left[\Phi_p \times \tanh\left(\frac{1}{\Phi_p}\right) \times (1 - \exp(\Phi_p))\right]\right)^{0.5} \tag{25}$$

where the aridity index (Φ_p) is defined as $\mathrm{ET}_{\mathrm{ref}}/P$. In SWEO, a 3-month moving average of the aridity index is incorporated to capture the cumulative effects of aridity over time. This accounts for the moisture conditions of preceding months and ensures that a single dry month does not immediately reduce $\mathrm{ET}_{\mathrm{ref}}/P$. Therefore, the SWEO's aridity index is defined as follows:

$$\Phi_p = \max\left(\Phi_p^t, \frac{1}{3} \times \sum_{i=0}^{2} \Phi_p^{t-i}\right) \tag{26}$$

The SWEO model compares actual ET from remote sensing data ($\mathrm{ET}_{\mathrm{act}}$) with the theoretical Budyko estimate ($\mathrm{ET}_{\mathrm{act}}^{\mathrm{budyko}}$). Pixels where $\mathrm{ET}_{\mathrm{act}}^{\mathrm{budyko}}$ exceeds the $\mathrm{ET}_{\mathrm{act}}$ represent land use and agro-ecosystems where ET can be fully explained by local rainfall. These so-called green pixels are neither irrigated nor receive water from flooding, groundwater interflow, or seepage. On the other hand, if $\mathrm{ET}_{\mathrm{act}}$ exceeds $\mathrm{ET}_{\mathrm{act}}^{\mathrm{budyko}}$, an additional water source besides rainfall must be present. These are the so-called blue pixels. The difference between $\mathrm{ET}_{\mathrm{act}}^{\mathrm{budyko}}$ and $\mathrm{ET}_{\mathrm{act}}$ also gives a first indication of the total amount of water supply from non-rainfall sources.

2.4.5. Step 5: calculation of rainfall runoff and sub-basin calibration using discharge time series

This step focuses on estimating the bulk runoff from each sub-basin. The soil infiltration process represents how precipitation contributes to surface and subsurface flow within a catchment, ultimately leading to river discharge. This step consists of two sub-steps. First, the runoff from rainfall is determined for each pixel using initial estimates of local infiltration processes. Second, the aggregation of runoff at sub-basin scale is tuned with observed river discharge time series.

Pixel-based rainfall runoff: The rainfall runoff per pixel ($\mathrm{RR}_{\mathrm{pix}}$) is approximated by using a modified version of the well-established soil conversation service (SCS) curve number. Infiltration properties are made dynamic according to soil moisture deficit and vegetation properties (Schaake *et al.* 1996), and the static curve numbers are thus replaced; see Hessels *et al.* (2022) for more information. SWEO divides the SCS curve into two components: one representing runoff generated by rainfall and the other representing runoff from snowmelt. This separation is necessary because meltwater is released differently over the month compared with precipitation. Rainfall intensity, which strongly controls runoff generation, can be approximated as the total monthly rainfall divided by the number of rainy days in that month. In contrast, snowmelt is assumed to be uniformly distributed over the month, resulting in a lower effective intensity and therefore reduced surface runoff. The two components are then summed, and the resulting equation is given as follows:

$$\mathrm{RR}_{\mathrm{pix}} = \frac{{R_{\mathrm{net}}^d}^2}{R_{\mathrm{net}}^d + S} \times \mathrm{RD} + \frac{{S_{m,\mathrm{net}}^d}^2}{S_{m,\mathrm{net}}^d + S} \times \mathrm{NOD} \tag{27}$$

Downloaded from iwaponline.com/jwcc/article-pdf/17/9/2484/1638061/jwc2026225.pdf
by Delft University of Technology user

where R^d_{net} represents the average daily rainfall and is defined as follows:

$$R^d_{\text{net}} = \frac{P - S_f}{\text{RD}} \tag{28}$$

$S^d_{m,\text{net}}$ represents the average daily snowmelt and is defined as follows:

$$S^d_{m,\text{net}} = \frac{S_m}{\text{NOD}} \tag{29}$$

The parameter S represents the maximum potential infiltration or retention before runoff begins. A lower S means less infiltration and more runoff and *vice versa*. It is defined as follows:

$$S = K_{\text{sat}} \times (\theta_{\text{sat}} - \theta_{\text{act}}) \times \psi \tag{30}$$

where K_{sat} is the saturated vertical hydraulic conductivity of the soil (mm day^{-1}) and ψ is the empirical enhancement factor for infiltration (–).

Soils with higher permeability (K_{sat}) facilitate greater water infiltration. SWEO adjusts the infiltration factor by utilizing the VC and terrain slope as proxies for the presence of roots and biological activity with an improved soil structure. Dense vegetation supports a more developed root system, which enhances soil porosity and promotes infiltration (Pingping *et al.* 2013). Additionally, in flatter terrains, surface runoff is reduced, which enhances infiltration. At steeper slopes, the volume of surface runoff increases while infiltration decreases (Fox *et al.* 1997). To incorporate these effects within SWEO, the empirical infiltration factor (ψ) is defined as follows:

$$\psi = (\text{VC} \times a + b) \times (1 - 0.5 \times \sin(s)/\sin(45^\circ)) \tag{31}$$

where s is the slope of the terrain (degrees) and 'a' and 'b' are calibration coefficients (by default a = 14, b = 6) (–).

The partitioning of precipitation and applied water into surface runoff versus infiltration is a complex process influenced by numerous interdependent factors and governed by nonlinear dynamics. Since hydraulic properties of sub-soil properties are often difficult to measure directly, any regional scale hydrological model has challenges to model the partitioning between surface runoff and deep percolation accurately (Morbidelli *et al.* 2018). It is therefore commonly accepted to calibrate system properties 'a' and 'b' from inverse modelling (Ha *et al.* 2018).

Sub-basin calibration of rainfall runoff: Surface runoff may undergo infiltration and percolation when traversing as overland flow towards the river. This conveyance effect reduces the total surface runoff reaching the river. This transport effect cannot be solved by the calibration coefficient 'a' and 'b' only. Therefore, the exclusive application of the standard surface runoff equation can produce unrealistic results, potentially leading to an imbalanced water budget.

To address this scale dependent issue, river discharge time series are used for the internal calibration of surface runoff. This calibration uses the SWEO estimated discharge at the catchment outlet and the available measured discharge data. The calibration is based on the concept that water reaches the river through two primary pathways, each characterized by a distinct lag time. The first is surface runoff or the 'fast component', which consists of water that flows overland directly to the river without infiltrating or percolating into the soil. This rapid movement is driven by factors like precipitation intensity, limited surface infiltration capacity, and sloping terrain. A discharge time series characterized by numerous fluctuations and zero flow during dry periods represents a sub-basin where the fast runoff component is the dominant driver.

The second pathway to feed rivers, involves subsurface flow, where water infiltrates into the soil, percolates into the groundwater system, and eventually reaches the river through baseflow or interflow. Baseflow refers to the slow drainage flow from groundwater into the river. Interflow describes water moving laterally through the shallow partially unsaturated subsurface toward the river, often occurring in hilly geographies. In the SWEO model, baseflow and interflow are represented as a single combined term. A hydrograph with limited response to rainfall indicates a sub-basin where the slow groundwater runoff component is dominant.

To achieve the separation into a slow and fast river component, a digital filtering approach is employed. This method can be applied to both daily and monthly time series data and is used to determine the baseflow of a sub-basin ($Q^{\text{sb}}_{\text{base}}$). A

Downloaded from iwaponline.com/jwcc/article-pdf/17/9/2484/1638061/jwc2026225.pdf
by Delft University of Technology user

disturbing factor is the regulation of river flow by human interventions. The river discharge must therefore be adjusted to represent natural conditions. The natural river discharge ($R^{sb}_{out,nat}$) is defined as the river discharge under conditions where no water is allocated for irrigation ($Q^{irr,sb}_{sws}$), canal flows (C^{sb}_{in}), and surface water storage of reservoirs (ΔS^{sb}_{sw}):

$$R^{sb}_{out,nat} = R^{meas,sb}_{out} + \Delta S^{sb}_{sw} + Q^{irr,sb}_{sws} - C^{sb}_{in} \tag{32}$$

A preliminary estimate of $Q^{irr,sb}_{sws}$ is obtained from the initial calculation of water supply from non-rainfall sources, using the Budyko principle applied in Step 4. Only pixels corresponding to irrigated areas are considered, as these are directly influenced by human activity and classified as non-natural. Land-use data identify croplands, while Budyko-based estimates distinguish between rainfed and irrigated areas.

The separation algorithm used by this filtering approach can be expressed by the following equation (Smakhtin 2001; Hughes *et al.* 2003):

$$Q^{sb,t}_{runoff} = \alpha \times Q^{sb,\,t-1}_{runoff} + \beta \times (1+\alpha)(R^{sb,t}_{out,\ nat} - R^{sb,t-1}_{out,\,nat}) \tag{33}$$

$$Q^{sb}_{base} = R^{sb}_{out,nat} - Q^{sb}_{runoff} \tag{34}$$

Q^{sb}_{runoff} is the fast runoff component of the sub-basin under natural river discharge conditions, and Q^{sb}_{base} indicates the baseflow component of the sub-basin. The parameters α and β serve as separation parameters. The parameter α varies within the range of 0–1, whereas β ranges from 0 to 0.5. The baseflow component Q^{sb}_{base} is constrained such that it cannot be negative or exceed the total natural river flow Q^{sb}_{nat}.

In the case of different upstream to downstream sub-basins, Q_{base} and Q_{runoff} from the upstream discharge measurement should be used so that each sub-basin has its own explicit separation. Upstream contributions are subtracted to isolate the fast runoff and baseflow of the current sub-basin:

$$Q^{sb}_{runoff} = Q^{sb,total}_{runoff} - Q^{sb,\,upstream}_{runoff} \tag{35}$$

$$Q^{sb}_{base} = Q^{sb,total}_{base} - Q^{sb,\,upstream}_{base} \tag{36}$$

Figure 3 presents an example of fast runoff and baseflow separation using the described filtering approach for a sub-basin in the Aconcagua Basin.

The total sub-basin volume of fast runoff (Q^{sb}_{runoff}), as derived using the filtering method based on the estimated natural discharge, can be directly related to the total sub-basin volume of surface runoff (RR^{sb}) for the entire sub-basin.

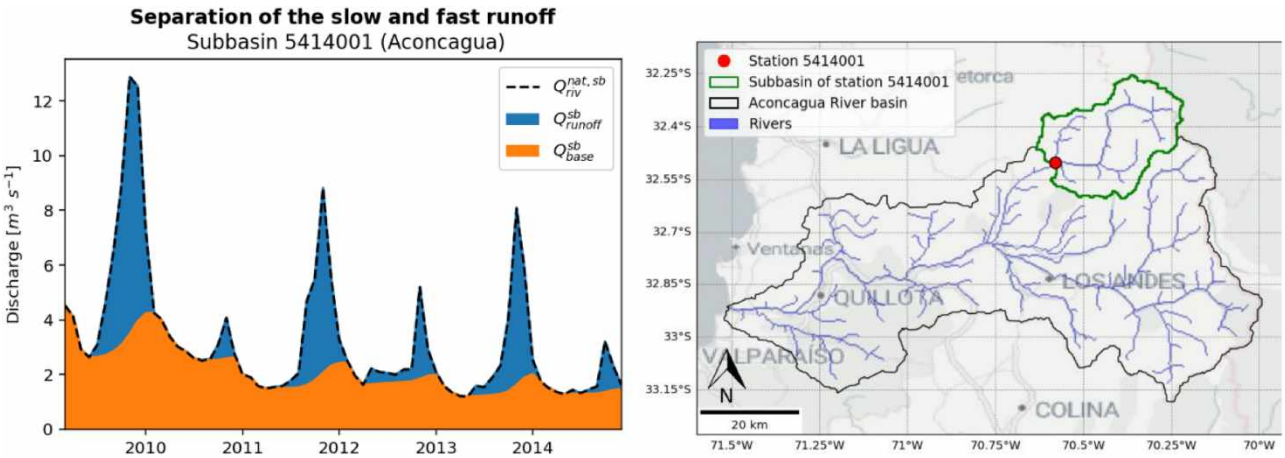


Figure 3 | Separation of natural river discharge into fast and slow runoff components at a monthly time step for a sub-basin of the Aconcagua River.

Downloaded from iwaponline.com/jwcc/article-pdf/17/9/2484/1638061/jwc2026225.pdf
by Delft University of Technology user

Consequently, RR^{sb} can be utilized to correct the pixel-scale surface runoff estimates (RR^{pix}) by applying a correction factor for conveyance losses.

During most months, RR^{sb} is lower than RR^{sb}_{pix}. In this situation the degree of infiltration along the flow path is assumed to increase with the distance a runoff pixel must travel to reach the river. Therefore, the correction factor is modelled as an exponential function of the pixel distance to the river. In the exceptional cases where RR^{sb} is higher than RR^{sb}_{pix}, which typically can occur during dry months, a bias correction over the sub-basin is applied. The corrected surface runoff at the pixel scale is therefore computed using the following equation:

$$RR = \begin{cases} RR_{pix} \times CORR^{\omega}, & RR^{sb} < RR^{sb}_{pix} \\ RR_{pix} \times \dfrac{RR^{sb}}{RR^{sb}_{pix}}, & RR^{sb} \geq RR^{sb}_{pix} \end{cases} \tag{37}$$

Here, CORR is a correction coefficient calibrated such that the total surface runoff for the sub-basin aligns with the total fast runoff volume (Q^{sb}_{runoff}). ω represents the number of grid cells that surface runoff must travel before reaching the river network.

2.4.6. Step 6: calculation of percolation and capillary rise

In this step, the estimation of vertical water fluxes between the upper and lower model layer is addressed, i.e., capillary rise and percolation. Capillary rise ($q_{\uparrow}$) refers to the upward movement of water from the groundwater table into the unsaturated zone driven by capillary forces. It is first estimated using an empirical approach to approximate this upward flux. Subsequently, percolation ($q_{\downarrow}$) is derived by closing the soil water balance for non-irrigated pixels. For irrigated areas, $q_{\downarrow}$ is instead determined through spatial and temporal interpolation of the percolation coefficient, ensuring consistency across varying irrigation conditions.

Capillary rise: Inspired by FAO (Ayers & Westcot 1985), capillary rise ($q_{\uparrow}$) is approximated by using the following empirical equation (Hessels *et al.* 2022):

$$q_{\uparrow} = \begin{cases} K_{sat,cap} \times (-0.175 \times \log(GWD_{rz}) + 0.25) \times NOD, & GWD_{rz} < GWD_{rz,max} \\ 0, & GWD_{rz} \geq GWD_{rz,max} \end{cases} \tag{38}$$

where $K_{sat,cap}$ is the saturated hydraulic conductivity specific to capillary rise, as default defined as 0.5 times K_{sat} to account for partial moisture saturation (mm day^{-1}) and GWD_{rz} is the depth between the root zone (H_{rz}) and the groundwater level (H_{gw}) (m).

The $q_{\uparrow}$ cannot be negative and is set to zero if GWD_{rz} exceeds the maximum groundwater depth (GWD_{max}) at which capillary rise occurs. The default SWEO value for GWD_{max} is 1 m; however, it may vary depending on land use. Additionally, $q_{\uparrow}$ is limited by the transpiration rate and cannot exceed it.

Percolation: Percolation ($q_{\downarrow}$) is a vertical Darcian flux in the vadose zone and is challenging to compute purely analytically due to the complexity of soil hydraulic properties and nonlinear dependence of flux on soil moisture (e.g., Rodrigues *et al.* 2024). Ahmad *et al.* (2002) nicely demonstrated the space and timescales of Darcian fluxes in irrigated cotton–wheat and rice–wheat cropping systems in Pakistan.

To avoid the dependency on complicated soil physical properties, SWEO estimates percolation by closing the water balance for the green water pixels identified in Step 4. For these pixels, a simplified water balance, as illustrated in Figure 4, is applied. In this simplified formulation, percolation becomes the sole unknown in the soil water balance, allowing it to be determined by closing the balance.

The empirical equation used to describe percolation from the bottom of the root zone in unsaturated soils is taken from the HBV model (Bergström 1995). Since percolation for green pixels is determined by closing the simplified water balance, these percolation values can also be used to estimate the percolation coefficient (δ) for those pixels:

$$q_{\downarrow} = P + q_{\uparrow} - I - ET - RR - \Delta S_{snow} - \Delta S_{\theta} = K_{sat} \times (\theta_{act}/\theta_{sat})^{\delta} \times NOD \tag{39}$$

Downloaded from iwaponline.com/jwcc/article-pdf/17/9/2484/1638061/jwc2026225.pdf
by Delft University of Technology user

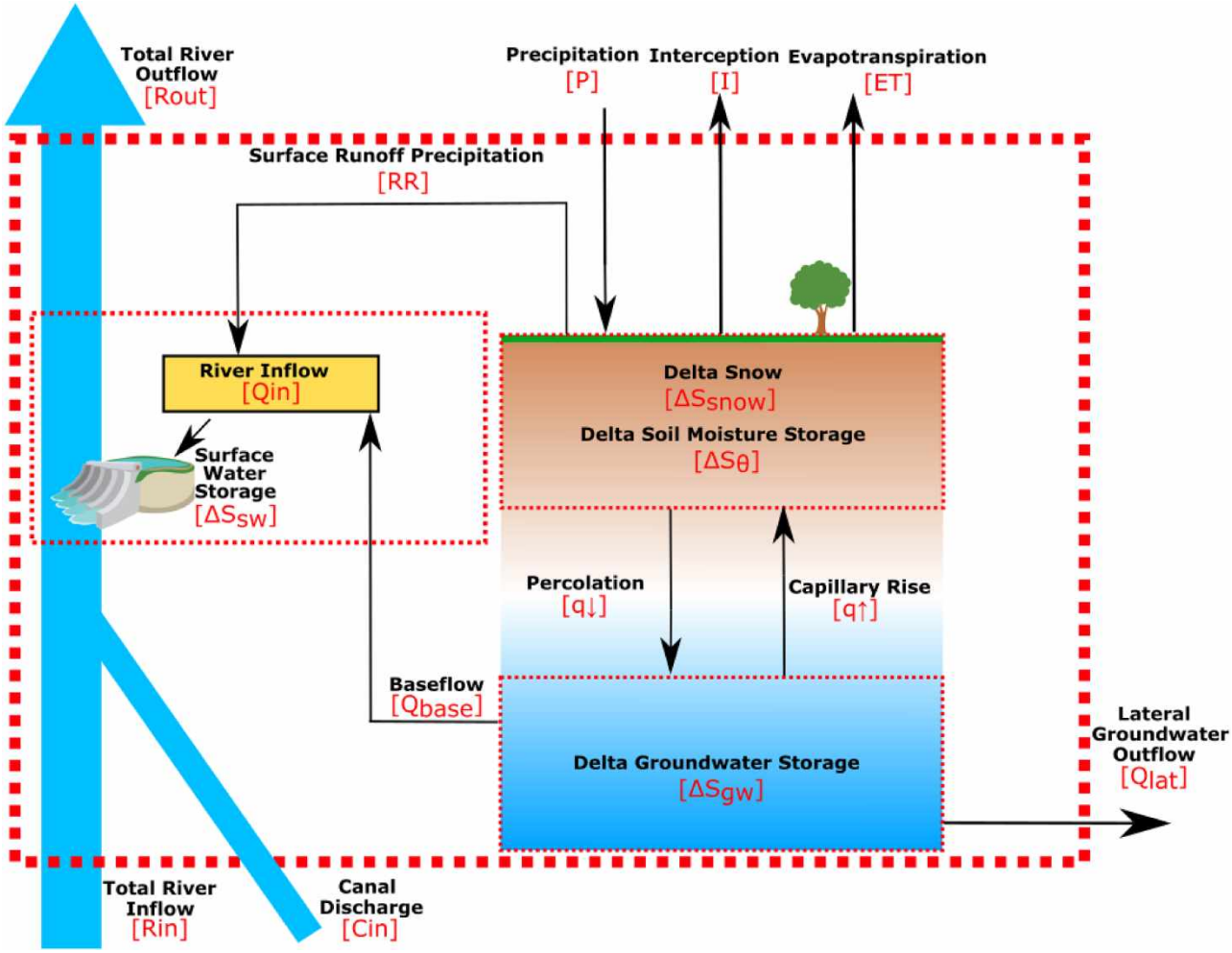


Figure 4 | Simplified soil water balance for green water pixels that can be used to infer spatial calibration of percolation.

The dimensionless δ defines the sensitivity of the percolation rate to soil moisture content. This coefficient is constrained to values between 1 and 5. The value of δ reacts to spatial variability of soil structure and soil physical properties.

This solution for calibrating percolation as a residual term of the soil water balance is one of the unique features of SWEO and provides strategic information for groundwater recharge. To determine the coefficient for the blue pixels, temporal and spatial interpolation of δ will be applied. This will be addressed in two steps.

First, the average δ per month across multiple years will be determined. The value of δ can be acquired from the same month in years when the pixel was classified as a green pixel. Second, the remaining data gaps of δ will be filled from spatial interpolation.

For pixels consisting of water bodies (lakes, reservoirs, rivers), percolation is computed differently. River percolation occurs when the river water level (H_{riv}) exceeds the groundwater head (H_{gw}). The vertical difference between the water surface level of the canal and the water table significantly influences percolation losses. By the absence of monthly water level information, although Surface Water and Ocean Topography (SWOT) altimeter can provide these data for selected rivers (Nair *et al.* 2022), the following simplified equation is applied:

$$q_{\downarrow} = \begin{cases} \emptyset \times K_{sat} \times \text{NOD}, & H_{gw} < H_{riv} \\ 0, & H_{gw} \geq H_{riv} \end{cases} \tag{40}$$

where $\emptyset$ represents a reduction factor of K_{sat} due to additional hydraulic resistance from the riverbed due to sedimentation. River pixels are delineated on a monthly basis by routing the components $P - \text{ET} - I - Q_{lat} - \Delta S_{tot}$ using a flow direction map. The default value for $\emptyset$ is 0.1.

Downloaded from iwaponline.com/jwcc/article-pdf/17/9/2484/1638061/jwc2026225.pdf
by Delft University of Technology user

2.4.7. Step 7: second partitioning of ET into ET_{green} and ET_{blue} for renewable water and allocations

The assessment of renewable water resources is a key output of SWEO. Basically renewable water is the difference between P minus I and ET of land surfaces that directly return soil moisture back in the atmosphere. Hence, the separation of ET into ET_{green} is essential for renewable water resources. ET_{blue} is essential for assessing the occurrence of non-rainfall water supply. A more precise distinction between green and blue water pixels can be achieved from modelling the root zone soil water balance under rainfed and irrigation conditions separately, and this approach is similar to Mekonnen & Hoekstra (2011) and is more comprehensive than using Budyko theorem applied in Step 4. However, because it requires estimates of percolation and capillary rise, this theorem can only be applied after Step 6.

To calculate this separation, the methodology outlined in the integrated water flow model demand calculator (IDC) is employed (Dogrul *et al.* 2011). This model provides a comprehensive and accurate framework for estimating ET_{blue} across various contexts, including agricultural irrigation. For distinguishing between green and blue ET, the IDC model utilizes a green water storage bucket concept. This bucket is replenished by net rainfall and capillary rise and depleted through percolation originating from rainfall. This percolation term is based on the ratio (α_p) between the soil moisture content derived from the green water storage bucket (θ_p) and the actual soil moisture content (θ_{act}) incorporating all types of water supplies:

$$\alpha_p^t = \frac{\theta_p^t}{\theta_{act}^t} \tag{41}$$

where the green water storage bucket is defined as:

$$\theta_p^t = \text{MAX}((S_p^{t-1} + P^t - I^t - \text{RR}^t - \Delta S_{snow}^t), 0)/T_{top} \tag{42}$$

In this equation, S_p^{t-1} represents the green water storage bucket from the previous timestep.

Since the initial green water storage (S_p^{-1}) is unknown, the initial ratio α_p must be defined by the user in order to get the initial green water storage bucket. The initial ratio value depends on the season in which the SWEO model is initialized. If the model starts during the rainy season, α_p is close to 1, whereas during the dry season, it is close to 0. This initial ratio is then used to compute θ_p^t by multiplying the ratio by the θ_{act}.

In the IDC model, α_p is constrained between 0 and 1 and is used to partition ET and $q\downarrow$ into components attributable to rainfall (green):

$$ET_{green}^t = \alpha_p^t \times ET^t \tag{43}$$

Here, ET_{green} is the ET attributable to rainfall. The percolation and evapotranspiration components attributable to rainfall are subsequently used to compute the green water storage bucket for the current timestep. Finally, the ET_{blue} can be determined by subtracting the ET_{green} term from the ET:

$$ET_{blue} = ET - ET_{green} \tag{44}$$

The IDC method also introduces a new classification of green and blue pixels, where pixels with $ET_{blue} > 0$ are classified as blue. This new classification is subsequently applied using the methodology defined in step 6. Accordingly, percolation is recomputed by repeating Equations (39) and (40).

2.4.8. Step 8: calculate groundwater withdrawal and surface water supply per sub-basin

This step focuses on determining the groundwater withdrawal (Q_{gw}^{sb}) and surface water supply (Q_{sws}^{sb}) for each sub-basin. Withdrawal refers to the volume of water extracted from the source. This volume differs from the supply ultimately delivered to each pixel, as it reflects conveyance and distribution losses.

In the previous steps, ΔS_{gw}, Q_{base}, and $q_{\downarrow}$ are all calibrated at a (sub)basin scale using the river discharge. Therefore, estimating total water supply at the sub-basin level provides greater accuracy than performing the estimation on a pixel basis

Downloaded from iwaponline.com/jwcc/article-pdf/17/9/2484/1638061/jwc2026225.pdf
by Delft University of Technology user

directly. The Q_{gw}^{sb} for a sub-basin can be determined by closing the groundwater water balance:

$$Q_{gw}^{sb} = q_{\downarrow}^{sb} - q_{\uparrow}^{sb} - \Delta S_{gw}^{sb} - Q_{lat}^{sb} - Q_{base}^{sb} \tag{45}$$

with the bulk groundwater withdrawal Q_{gw}^{sb} being determined, the Q_{sws}^{sb} remains the only unknown variable in the soil water balance at the sub-basin scale. By closing this soil water balance, Q_{sws}^{sb} can be determined and is expressed as follows:

$$Q_{sws}^{sb} = Q_{sw}^{sb} - RR_{irr}^{sb} = P^{sb} - I^{sb} - ET^{sb} + Q_{gw}^{sb} + q_{\uparrow}^{sb} - q_{\downarrow}^{sb} - \Delta S_{\theta}^{sb} - \Delta S_{snow}^{sb} - RR^{sb} \tag{46}$$

2.4.9. Step 9: breakdown of groundwater and surface water supply per pixel using proxies

Step 8 estimates the bulk Q_{gw}^{sb} and Q_{sws}^{sb} volumes for each sub-basin as an intermediate step. These aggregated volumes are subsequently disaggregated to the pixel level using a set of spatial proxies. The proxies represent monthly factors that influence whether groundwater or surface water is more likely to supply ET_{blue} pixels.

The proxies capture spatial and temporal drivers of water source selection, including land use, proximity to water sources, resource availability, and seasonal variability. Based on these indicators, the bulk sub-basin withdrawals are distributed across pixels to derive pixel-specific estimates of monthly groundwater and surface water contributions.

By default, the following five proxies are considered:

Proxy 1: Land use
Proxy 2: Distance to surface water source
Proxy 3: Depth towards the groundwater source
Proxy 4: Amount of 'negative' base/interflow
Proxy 5: Variation in ET over the growing season

Each proxy assigns a relative weight that distinguishes between groundwater and surface water as the likely source supplying ET_{blue} pixels. A relatively lower weight indicates a higher probability that the supplied water originates from groundwater rather than surface water.

These five proxies represent default indicators used in SWEO. Additional proxies may also be incorporated when they provide relevant information for distinguishing groundwater and surface water contributions in a specific region. The default individual proxies are defined as follows:

Proxy 1: Land use. Q_{sws} is assumed to occur primarily in the land-use classes irrigated land, floodplains (including wetlands), and urban areas. These classes may also have conjunctive use of groundwater. For all other land-use classes, the water supply is assumed to originate from groundwater sources, including GDEs. This proxy generates a Boolean map, where a value of 1 represents areas that may be supplied by surface water, while 0 indicates land-use types supplied exclusively by groundwater.

$$\text{Proxy 1} = \begin{cases} 1, & \text{land use} = \text{irigated} \\ 0, & \text{land use} \neq \text{irigated} \end{cases} \tag{47}$$

Proxy 2: Distance to surface water. The proximity of irrigated fields to surface water bodies (e.g., rivers or reservoirs) influences the likelihood of surface water irrigation. Fields located close to surface water are more likely to use surface water as an irrigation source. In addition, the relative elevation difference between the field and the surface water body affects accessibility. This proxy is defined as follows:

$$\text{Proxy 2} = (1/(\text{DIST}/10000 + (\text{MAX}(\text{HAND} - 10,\ 0)/10)) \tag{48}$$

where HAND represents the height above the nearest drain in metres and DIST is the nearest distance to surface water in metres. Both variables may vary monthly, reflecting seasonal conditions in which some rivers may run dry. Proxy 2 is limited between 0.1 and 1. The formulation implies that the proxy value gradually decreases when the horizontal distance to surface water exceeds approximately 10 km or when the vertical elevation difference exceeds about 10 m, reflecting the reduced likelihood of surface water being used for irrigation under these conditions. These threshold values are indicative and may vary

Downloaded from iwaponline.com/jwcc/article-pdf/17/9/2484/1638061/jwc2026225.pdf
by Delft University of Technology user

between regions depending for example on the scale and design of local irrigation canal systems. In areas with limited canal or conveyance systems, the effective distance over which surface water can be supplied may be considerably smaller.

Proxy 3: Depth towards the groundwater source. Groundwater withdrawal becomes more favourable when the groundwater depth (GWD) is relatively shallow. When the groundwater table is closer to the surface than the level of nearby surface water bodies, groundwater becomes a more attractive source in terms of cost, water quality, and reliability. This proxy is represented by the following equation:

$$\text{Proxy 3} = \begin{cases} 1, & \text{HAND} < \text{GWD} \\ \alpha + (1-\alpha) \times \text{GWD}/\text{HAND}, & \text{else} \end{cases} \tag{49}$$

where GWD is groundwater depth and α is a calibration parameter (default α = 0.02). Proxy 3 is limited between α and 1.

Proxy 4: Redistribution of groundwater surplus. The groundwater balance based on the current fluxes and storage states provides an initial estimate of potential groundwater availability at the pixel scale. In this balance, groundwater withdrawals represent the only unknown component. By assuming that the entire water supply originates from groundwater, it is possible to evaluate whether groundwater resources alone can meet the water demand.

Under this assumption, the total groundwater surplus or deficit per pixel (RES_{gw}) can be calculated as follows:

$$\text{RES}_{\text{gw}} = q_{\downarrow} - q_{\uparrow} - \text{ET}_{\text{blue}} - \Delta S_{\text{gw}} - Q_{\text{lat}} \tag{50}$$

The resulting RES_{gw} value for each pixel can be either positive or negative. By routing the RES_{gw} values according to the drainage direction, the aggregated RES_{gw} flux at the river can likewise be positive or negative. All the upstream pixels contributing to that river segment are assigned the routed value, producing the $\text{RES}_{\text{gw}}^{\text{routed}}$ parameter.

Pixels with a positive $\text{RES}_{\text{gw}}^{\text{routed}}$ value indicate that sufficient groundwater is available in that part of the basin to meet the total water demand (i.e., groundwater surplus). Conversely, negative $\text{RES}_{\text{gw}}^{\text{routed}}$ values indicate that groundwater alone cannot satisfy the total water demand (i.e., groundwater deficit). In areas with groundwater deficit, these deficit areas should receive higher priority in the redistribution of $Q_{\text{sws}}^{\text{sb}}$, as they are more likely to rely on surface water, resulting in higher proxy values. To convert $\text{RES}_{\text{gw}}^{\text{routed}}$ into a proxy representing the likelihood of surface water use, proxy 4 is defined as follows:

$$\text{Proxy 4} = \begin{cases} 0.2 - 0.8 \times \text{RES}_{\text{gw}}^{\text{routed}}/\text{ET}_{\text{blue}}^{\text{routed}}, & \text{RES}_{\text{gw}}^{\text{routed}} < 0 \\ 0.2, & \text{else} \end{cases} \tag{51}$$

where $\text{ET}_{\text{blue}}^{\text{routed}}$ is the routed ET_{blue} using the same routing procedure as for the RES_{gw}.

Finally, a Gaussian filter is applied to proxy 4 to account for the fact that groundwater flow in reality does not strictly follow these drainage directions. This filtered proxy will therefore represent the groundwater flow conditions of the surrounding area more realistically. Proxy 4 is limited between 0.2 and 1.

Proxy 5: Variation in ET over the growing season. Many irrigated areas experience water scarcity by design. Protective irrigation is meant to provide a minimum amount of surface water Q_{sw} to protect crops from adverse effects of soil moisture deficiency (Jurriëns & Wester 1994). Under such circumstances, canal water allocation is low and insufficient for high water-demand crops. Consequently, pixels irrigated with groundwater typically experience higher ET over the growing season compared with pixels relying solely on surface water. This also occurs when canal water supply is modest, and farmers mentally believe that water deficit prevails. The hypothesis underlying proxy 5 is that pixels with accumulated seasonal ET above the average value are more likely to represent groundwater contributions.

Based on the annual distributions of total ET_{blue} values, pixels with the highest ET_{blue} are assigned the lowest values for Proxy 5, indicating a higher probability of groundwater supply. This proxy is calculated as follows:

$$\begin{cases} 0.2, & \text{PER}_{\text{ET}_{\text{blue}}} > \text{LIM}_{\text{high}} \\ 1.0 - 0.8 \times \left(\dfrac{\text{PER}_{\text{ET}_{\text{blue}}} - \text{LIM}_{\text{low}}}{\text{LIM}_{\text{high}} - \text{LIM}_{\text{low}}} \right), & \text{LIM}_{\text{low}} > \text{PER}_{\text{ET}_{\text{blue}}} > \text{LIM}_{\text{high}} \\ 1.0, & \text{else} \end{cases} \tag{52}$$

Downloaded from iwaponline.com/jwcc/article-pdf/17/9/2484/1638061/jwc2026225.pdf
by Delft University of Technology user

Here, PER_{ETblue} represents the percentile of annual ET_{blue} for a given pixel relative to all pixels. LIM_{low} and LIM_{high} define the percentile bounds corresponding to the lowest and highest proxy values, respectively (default 2.5 and 50). Since Proxy 5 is based on annual ET_{blue}, it remains constant throughout the year.

Total proxy: The total monthly proxy is calculated as the product of all individual proxies:

$$\text{PROXY} = \text{Proxy 1} \times \text{Proxy 2} \times \text{Proxy 3} \times \text{Proxy 4} \times \text{Proxy 5}^{y} \tag{53}$$

By default, all proxies contribute equally to this combined PROXY. The relative influence of individual proxies can be adjusted by applying an exponent to a specific proxy term. Higher exponents increase the relative importance of that proxy in determining the spatial allocation of water sources.

Low PROXY values indicate a high likelihood of groundwater supply. To avoid unrealistically small surface water allocations, very small proxy values are filtered using:

$$\text{PROXY}_{\text{LIMIT}} = \overline{\text{PROXY}} - (\text{PROXY}_{99} - \overline{\text{PROXY}}) \tag{54}$$

where $\overline{\text{PROXY}}$ is the average PROXY value (–) and PROXY_{99} is the 99th percentile of the PROXY values (–).

Pixels with PROXY < PROXYLIMIT are set to zero:

$$\text{PROXY} = \begin{cases} 0, & \text{PROXY} < \text{PROXY}_{\text{LIMIT}} \\ \text{PROXY}, & \text{else} \end{cases} \tag{55}$$

Allocation of surface water supply: The PROXY values represent relative likelihood indicators within each sub-basin. After normalization, the allocation of surface water therefore depends on the relative differences between pixels rather than the absolute proxy values. Consequently, even pixels with relatively low proxy values may receive a larger share of surface water when the overall proxy distribution within the sub-basin is low.

To generate a proxy fraction map per sub-basin, the PROXY is divided by the sum of PROXY values over a sub-basin (PROXY^{sb}_{tot}). This pixel-based map is used to allocate the total net surface water supply across the sub-basin using the following formula:

$$Q_{sws} = Q^{sb}_{sws} \times \frac{\text{PROXY}}{\text{PROXY}^{sb}_{tot}} \tag{56}$$

Since the total Q_{sws} cannot exceed ET_{blue} and the corresponding Q^{sb}_{sws} must match the value determined in step 8, any excess ET_{blue} must be reallocated to other pixels. This process is iterative, continuing until the remaining not allocated water supply (positive values of $Q_{sws} - ET_{blue}$) is distributed among pixels in a way that honours the proxies, ensures the bulk Q^{sb}_{sws} remains consistent with step 8, and ensures Q_{sws} does not exceed ET_{blue}.

After completing the iterative process, Q_{sws} is determined, and the pixel-based Q_{gw} can be calculated using the groundwater balance:

$$Q_{gw} = \text{ET} + I - P - Q_{sws} - q_{\uparrow} + q_{\downarrow} + \Delta S_{\theta} + \Delta S_{snow} + \text{RR} \tag{57}$$

2.4.10. Step 10: calculate surface water withdrawal and baseflow per pixel

The final step in the SWEO water balance is to compute the surface water withdrawal (Q_{sw}) and irrigation runoff (RR_{irr}), and convert the sub-basin based Q^{sb}_{base}, derived from discharge measurements, into a pixel-based baseflow map (Q_{base}).

Surface water withdrawal and irrigation runoff. The surface water withdrawal (Q_{sw}) and irrigation runoff (RR_{irr}) are calculated using the runoff coefficient (C) and Q_{sws}. The runoff coefficient is an input parameter in the SWEO model and is defined based on irrigation type and the presence of bunds that restrict drainage. For flood irrigation, the runoff coefficient can reach values up to 0.3, whereas under micro-irrigation systems, it is substantially lower, typically around 0.03. The RR_{irr} can be determined by:

$$RR_{irr} = (Q_{sws} \times C)/(1 - C) \tag{58}$$

Downloaded from iwaponline.com/jwcc/article-pdf/17/9/2484/1638061/jwc2026225.pdf
by Delft University of Technology user

Q_{sw} is determined using the following equation:

$$Q_{sw} = Q_{sws} + RR_{irr} \tag{59}$$

Conversion of sub-basin based baseflow to pixel-based map. The pixel value of Q_{gw} is determined from proxies and not from the local groundwater balance. For this reason, Q_{base} can be approximated as a local residual term. As all other fluxes and states of this deeper groundwater balance, with the exception of lateral groundwater flow, have been determined at the pixel level in the preceding steps, Q_{base} can be refined as follows:

$$Q_{base} = q_{\downarrow} - q_{\uparrow} - Q_{gw} - \Delta S_{gw} - Q_{lat}^{sb} \tag{60}$$

A numerical groundwater flow model is required to more precisely differentiate this flow into Q_{base} and Q_{lat}. For a first level analysis of sub-basin water accounts, such detailed representation of these individual sub-processes is not required.

3. OPPORTUNITIES OF THE METHODOLOGY

The unique character of SWEO is the strictly sequential computational process with internal calibrations for annual and monthly storage changes, introduction of bias factors for annual ET, monthly snow cover, and monthly surface runoff (for wet season) and percolation coefficients (for dry season) based on measured hydrographs on a few locations. So uncertainty in certain geospatial input data is not propagated throughout the entire model and instead mass conservation principles are used to correct certain hydrological processes. It is thus untrue that uncertainty from different input data layers add up because of these automated corrections being built in. The use of globally available datasets ensures that the methodology can be applied consistently across diverse regions, supporting large-scale water accounting processing in the cloud. All input data layers are verifiable, and human manipulations of hydrological data are ruled out because they are not used.

Due to the high spatial detail of 100–250 m, the hydrological and anthropogenic water management process can be linked to land use and land cover. The latter is required for understanding economic, social, and ecosystem services from water resources. The monthly water flow path, fluxes, and benefits can be used directly for Sustainable Development Goal (SDG) reporting following indicators as for instance suggested by Karimi *et al.* (2015) and Van Ham *et al.* (2018).

The SWEO water accounting framework has been applied in multiple hydro-climatic regions. Earlier versions have been successfully implemented in the transboundary Indus Basin (Pakistan, India, Afghanistan, and China), major basins in Afghanistan, the Syr Darya Basin (Central Asia), the Irrawaddy Basin (Myanmar), the Jordan Basin and Mountain Aquifer (Palestine and Israel), and major basins in Chile. These applications demonstrate the practical applicability of the framework to assess water flow in river basins and interactions between soil water systems, network of surface waters, and aquifers.

The enhanced SWEO framework presented in this article is evaluated in a separate validation study applied to the Aconcagua Basin (Chile), Platte Basin (USA), and Madera Basin (USA). The companion paper assesses the performance of the methodology under different hydro-climatic conditions and compares the estimated groundwater fluxes with independent observations, providing an independent evaluation of the framework's reliability (Hessels *et al.* 2026).

4. LIMITATIONS OF THE METHODOLOGY

SWEO describes vertical and horizontal groundwater flows. The horizontal baseflow and lateral groundwater flow are calculated from groundwater balance surplus and deficits, not explicitly from routing of groundwater through unconfined aquifers. Net groundwater outflow across river basins water divides is currently copied from a single global groundwater flow model. As long as these net outflows remain relatively small, this approach is considered acceptable, but it is worthwhile to mention this as a limitation. Total volumes of baseflow and lateral flow are generally accurate at the sub-basin scale, though partitioning within individual pixels is less precise.

SWEO assumes that the spatial variability of ET is adequately captured by their respective input datasets. The introduction of ET bias corrections do not have impact on the spatial variability: all pixels get the same relative change. Hence, the spatial

Downloaded from iwaponline.com/jwcc/article-pdf/17/9/2484/1638061/jwc2026225.pdf
by Delft University of Technology user

variability of these products can introduce uncertainties, potentially leading to uncertainty in model outputs. Hence, the selection of certain ET data layers has influence on local soil water balances.

SWEO is globally applicable and relies exclusively on open-access satellite imagery, widely available GIS datasets, and the pressure head distribution and basin groundwater outflow from a global hydrological model (PCR-GLOBWB has been used in this case). Discharge measurements available at a few hydro-meteorological observation posts are sufficient to calibrate surface water outflow from delineated drainage areas. These river discharges serve two purposes: first, to refine GRACE-derived monthly groundwater storage values, and second, to provide information on the partitioning between rapid surface runoff and slower groundwater runoff. Future research will examine how water balances change in the absence of river discharge measurements. New satellite altimetry products could provide a promising alternative for river water levels and discharges. The current SWEO version does not incorporate altimeter-based water level measurements, but the increasing availability of such data, including from the SWOT satellite (Bhattacharjee *et al.* 2025), could make SWEO less dependent on available discharge measurements.

The SWEO methodology is based on the natural hydrological flow system. Withdrawals for domestic and industrial purposes cannot be captured by satellite observations, and population density maps are used as proxies to estimate these withdrawals, taking per capita water use from AQUASTAT. Similarly, managed aquifer recharge and discharges from sewerage systems are not included. Where such data are available from open source such as FAO's AQUASTAT, they can be incorporated to improve the accuracy of the water balance.

5. CONCLUSIONS

The arrival of 'water bankruptcy' requires urgent interventions in the water sector. The ongoing, unmanaged depletion of aquifers is collapsing important components of the hydrological system. Effective water management programs, such as SDG indicators, Integrated Water Resources Management, water footprint assessments, and the water-energy-food nexus, all rely on accurate water accounts as a foundation (Perry 2011), while the absence of critical data limits our understanding of ongoing processes (Molden 1997). Global data systems such as FAO's AQUASTAT have provided valuable information on water use and management over the past decades, but the data represent aggregated values for countries or at best for states. SWEO offers spatially distributed information that can be used to create reports by sub-aquifers and land-use categories.

SWEO represents a transparent, globally applicable, and scalable framework, building on a series of innovative spatial data solutions for specific hydrological processes. The method provides insight into key groundwater-related processes, including groundwater recharge, withdrawals, and the functioning of GDEs without the need to have access to *in situ* measurement programs or complex geo-hydrological system descriptions. By relying on open-access remote sensing datasets and simple water balance principles, the framework delivers spatially distributed information across large river basins with a favourable resolution of 100–250 m. The input data can be reviewed in case of discrepancies with physical observations and the system allows alternative spatial data layers to be used. SWEO is independent of human manipulations of water levels, discharges and withdrawals. Although SWEO does not simulate the detailed nonlinear dynamics of groundwater flow, it generates robust estimates of the degree of aquifer over-draft and sets safe withdrawals for sub-aquifers and local administrative boundaries. This helps responsible agencies with controlling declining groundwater table with undesirable consequences such as land subsidence and environmental droughts.

The methodology can be applied consistently across data-scarce river basins, and it automatically creates monthly and annual water accounts in the cloud. The results obtained from the SWEO methodology can be utilized to calculate a comprehensive list of water management indicators for climate resilience and water scarcity solutions. These indicators and data can be used to report renewable water resources, water storage requirements to survive dry years, water use by sector, beneficial water use, utilizable water, various types of water productivities, hydrological ecosystem services, sustainable water allocations, aquifers restoration, groundwater permits, reuse and recycling of water, need for non-conventional water resources, and more.

In summary, SWEO water accounting delivers a transparent, reproducible, and globally applicable approach to understanding basin-scale hydrology including groundwater resources. It can process large basins in a few days. This is currently not feasible from the existing UN groundwater databases and numerical groundwater simulation models. Despite its simplifications regarding groundwater flow, which is also its strength, it provides actionable insights into recharge and withdrawals that can directly inform policy and water management decisions worldwide.

Downloaded from iwaponline.com/jwcc/article-pdf/17/9/2484/1638061/jwc2026225.pdf
by Delft University of Technology user

FUNDING

This study did not receive support from any external funding sources.

DATA AVAILABILITY STATEMENT

Data cannot be made publicly available; readers should contact the corresponding author for details.

CONFLICT OF INTEREST

The authors declare there is no conflict.

REFERENCES

Ahmad, M. D., Bastiaanssen, W. G. M. & Feddes, R. A. (2002) Sustainable use of groundwater for irrigation: a numerical analysis of subsoil water flux, *Irrigation and Drainage*, **51** (3), 227–241. doi:10.1002/ird.59.

Ahmad, M. U. D. & Bastiaanssen, W. G. (2003) Retrieving soil moisture storage in the unsaturated zone using satellite imagery and bi-annual phreatic surface fluctuations, *Irrigation and Drainage Systems*, **17** (3), 141–161. doi:10.1023/A:1025101217521.

Ahmad, M. U. D., Bastiaanssen, W. G. M. & Feddes, R. A. (2005) A new technique to estimate net groundwater use across large irrigated areas by combining remote sensing and water balance approaches, Rechna Doab, Pakistan, *Hydrogeology Journal*, **13** (5), 653–664. doi:10.1007/s10040-004-0394-5.

Ayers, R. S. & Westcot, D. W. (1985) *Water Quality for Agriculture*, Vol. 29. Rome: Food and agriculture organization of the United Nations, p. 174.

Bastiaanssen, W. G. M. (2009) *Water accountants: de nieuwe generatie waterbeheercontroleurs*. Delft, The Netherlands: Technische Universiteit Delft.

Bastiaanssen, W. G., Allen, R. G., Droogers, P., D'Urso, G. & Steduto, P. (2007) Twenty-five years modeling irrigated and drained soils: state of the art, *Agricultural Water Management*, **92** (3), 111–125. doi:10.1016/j.agwat.2007.05.013.

Batchelor, C., Hoogeveen, J., Faurès, J. M. & Peiser, L. (2016) *Water Accounting & Auditing Guidelines: A Sourcebook*, 43. Rome, Italy: Food & Agriculture Org.

Bergström, S. (1995) The HBV model, Computer Models of Watershed Hydrology, edited by: Singh, VP.

Bhattacharjee, R., Dwivedi, S. B., Gaur, S., Chander, S. & Ohri, A. (2025) A review of the evolution of satellite radar altimetry for hydrological monitoring: water level and discharge estimation, *Physics and Chemistry of the Earth, Parts A/B/C*, **141** (1), 104039.

Biemans, H. (2012) *Water Constraints on Future Food Production*. Wageningen, The Netherlands: Wageningen University and Research.

Braden, H. (1985) Ein energiehaushalts-und verdunstungsmodell for wasser und stoffhaushaltsuntersuchungen landwirtschaftlich genutzer einzugsgebiete, *Mittelungen Deutsche Bodenkundliche Geselschaft*, **42** (S), 294–299.

Budyko, M. I. & Miller, D. H. (1974) *Climate and Life Academic Press*. New York: Academic Press, Orlando, USA.

Camberlin, P., Barraud, G., Bigot, S., Dewitte, O., Makanzu Imwangana, F., Maki Mateso, J. C., Martiny, N., Monsieurs, E., Moron, V., Pellarin, T. & Philippon, N. (2019) Evaluation of remotely sensed rainfall products over Central Africa, *Quarterly Journal of the Royal Meteorological Society*, **145** (722), 2115–2138. doi:10.1002/qj.3547.

Cheema, M. J. M., Immerzeel, W. W. & Bastiaanssen, W. G. M. (2014) Spatial quantification of groundwater abstraction in the irrigated Indus basin, *Groundwater*, **52** (1), 25–36. doi:10.1111/gwat.12027.

Condeça, J., Nascimento, J. & Barreiras, N. (2022) Monitoring the storage volume of water reservoirs using Google Earth Engine, *Water Resources Research*, **58** (3), e2021WR030026. doi:10.1029/2021WR030026.

De Graaf, I. E. M., Van Beek, L. P. H., Wada, Y. & Bierkens, M. F. P. (2014a) Dynamic attribution of global water demand to surface water and groundwater resources: effects of abstractions and return flows on river discharges, *Advances in Water Resources*, **64**, 21–33. doi:10.1016/j.advwatres.2013.12.002.

De Graaf, I. E. M., Sutanudjaja, E. H., Van Beek, L. P. H. & Bierkens, M. F. P. (2014b) A high resolution global scale groundwater model, *Hydrology & Earth System Sciences Discussions*, **19** (2), 823–837.

Dembélé, M. & Zwart, S. J. (2016) Evaluation and comparison of satellite-based rainfall products in Burkina Faso, West Africa, *International Journal of Remote Sensing*, **37** (17), 3995–4014. doi:10.1080/01431161.2016.1207258.

Dinku, T., Funk, C., Peterson, P., Maidment, R., Tadesse, T., Gadain, H. & Ceccato, P. (2018) Validation of the CHIRPS satellite rainfall estimates over Eastern Africa, *Quarterly Journal of the Royal Meteorological Society*, **144**, 292–312. doi:10.1002/qj.3244.

Dogrul, E. C., Kadir, T. N. & Chung, F. I. (2011) Root zone moisture routing and water demand calculations in the context of integrated hydrology, *Journal of Irrigation and Drainage Engineering*, **137** (6), 359–366. doi:10.1061/(ASCE)IR.1943-4774.0000306.

Donchyts, G., Baart, F., Winsemius, H., Gorelick, N., Kwadijk, J. & Van de Giesen, N. (2017) Earth's surface water change over the past 30 years, *Nature Climate Change*, **6** (9), 810–813.

Duan, Z. & Bastiaanssen, W. G. M. (2013) Estimating water volume variations in lakes and reservoirs from four operational satellite altimetry databases and satellite imagery data, *Remote Sensing of Environment*, **134**, 403–416. doi:10.1016/j.rse.2013.03.010.

Fox, D. M., Bryan, R. B. & Price, A. G. (1997) The influence of slope angle on final infiltration rate for interrill conditions, *Geoderma*, **80** (1–2), 181–194. doi:10.1016/S0016-7061(97)00075-X.

Downloaded from iwaponline.com/jwcc/article-pdf/17/9/2484/1638061/jwc2026225.pdf
by Delft University of Technology user

Fu, B. P. (1981) On the calculation of the evaporation from land surface, *Scientia Atmospherica Sinica*, **5** (1), 23.k.

Gerrits, A. M. J., Savenije, H. H. G., Veling, E. J. M. & Pfister, L. (2009) Analytical derivation of the Budyko curve based on rainfall characteristics and a simple evaporation model, *Water Resources Research*, **45** (4), W04403. doi:10.1029/2008WR007308.

Ha, L. T., Bastiaanssen, W. G., Van Griensven, A., Van Dijk, A. I. & Senay, G. B. (2018) Calibration of spatially distributed hydrological processes and model parameters in SWAT using remote sensing data and an auto-calibration procedure: a case study in a Vietnamese river basin, *Water*, **10** (2), 212. doi:10.3390/w10020212.

Hain, C. R., Crow, W. T., Mecikalski, J. R., Anderson, M. C. & Holmes, T. (2011) An intercomparison of available soil moisture estimates from thermal infrared and passive microwave remote sensing and land surface modeling, *Journal of Geophysical Research*, **116** (D15107). doi:10.1029/2011JD015633.

Hessels, T. M. (2015) *Comparison and Validation of Several Open Access Remotely Sensed Rainfall Products for the Nile Basin*. *MSc. Thesis*, Delft University of Technology, The Netherlands.

Hessels, T., Davids, J. C. & Bastiaanssen, W. (2022) Scalable Water Balances from Earth Observations (SWEO): results from 50 years of remote sensing in hydrology, *Water International*, **47** (6), 866–886. doi:10.1080/02508060.2022.2117896.

Hessels, T. M., Bastiaanssen, W. G. M., Stigter, T. Y., Davids, J. C., Schoups, G. & Perry, C. J. (2026) On the determination of pixel-based groundwater withdrawals using SWEO water accounting procedures. part 2: validation, *Journal of Water and Climate Change*.

Hofste, R. W. (2014) *Comparative Analysis among Near-Operational Evapotranspiration Products for the Nile Basin Based on Earth Observations*. *Master thesis*, Delft University of Technology, Delft, The Netherlands.

Hou, J., Van Dijk, A. I. J. M., Renzullo, L. J. & Larraondo, P. R. (2022) Glolakes: a database of global lake water storage dynamics from 1984 to present derived using laser and radar altimetry and optical remote sensing, *Earth System Science Data Discussions*, **2022**, 1–20.

Huang, Z., Hejazi, M., Li, X., Tang, Q., Vernon, C., Leng, G., Liu, Y., Döll, P., Eisner, S., Gerten, D. & Hanasaki, N. (2018) Reconstruction of global gridded monthly sectoral water withdrawals for 1971–2010 and analysis of their spatiotemporal patterns, *Hydrology and Earth System Sciences*, **22** (4), 2117–2133. doi:10.5194/hess-22-2117-2018.

Hughes, D. A., Hannart, P. & Watkins, D. (2003) Continuous baseflow separation from time series of daily and monthly streamflow data, *Water Sa*, **29** (1), 43–48.

Jurriëns, M. & Wester, P. (1994) *Protective Irrigation in India*, ILRI Annual Report, Wageningen, The Netherlands.

Kalbus, E., Reinstorf, F. & Schirmer, M. (2006) Measuring methods for groundwater–surface water interactions: a review, *Hydrology and Earth System Sciences*, **10** (6), 873–887. doi:10.5194/hess-10-873-2006.

Karimi, P., Bastiaanssen, W. G. & Molden, D. (2013) Water accounting plus (WA+)–a water accounting procedure for complex river basins based on satellite measurements, *Hydrology and Earth System Sciences*, **17** (7), 2459–2472. doi:10.5194/hess-17-2459-2013.

Karimi, P., Bastiaanssen, W. G. M., Sood, A., Hoogeveen, J., Bastidas-Obando, E. & Dost, R. (2015) Spatial evapotranspiration, rainfall and land use data in water accounting – part 2: reliability of water accounting results for policy decisions in the awash basin, *HESS*, **19**, 533–550.

Knipper, K., Anderson, M., Bambach, N., Melton, F., Ellis, Z., Yang, Y., Volk, J., McElrone, A. J., Kustas, W., Roby, M. & Carrara, W. (2024) A comparative analysis of OpenET for evaluating evapotranspiration in California almond orchards, *Agricultural and Forest Meteorology*, **355**, 110146. doi:10.1016/j.agrformet.2024.110146.

Kustas, W. & Anderson, M. (2009) Advances in thermal infrared remote sensing for land surface modeling, *Agricultural and Forest Meteorology*, **149** (12), 2071–2081. doi:10.1016/j.agrformet.2009.05.016.

Lee, H., Beighley, R. E., Alsdorf, D., Jung, H. C., Shum, C. K., Duan, J., Guo, J., Yamazaki, D. & Andreadis, K. (2011) Characterization of terrestrial water dynamics in the Congo Basin using GRACE and satellite radar altimetry, *Remote Sensing of Environment*, **115** (12), 3530–3538. doi:10.1016/j.rse.2011.08.015.

Le Maitre, D. C., Scott, D. F. & Colvin, C. (1999) A review of information on interactions between vegetation and groundwater, *WATER SA-PRETORIA*, **25**, 137–152.

Loomis, B. D., Felikson, D., Sabaka, T. J. & Medley, B. (2021) High-spatial-resolution mass rates from GRACE and GRACE-FO: global and ice sheet analyses, *Journal of Geophysical Research: Solid Earth*, **126** (12), e2021JB023024. doi:10.1029/2021JB023024.

Lubell, M., Blomquist, W. & Beutler, L. (2020) Sustainable groundwater management in California: a grand experiment in environmental governance, *Society & Natural Resources*, **33** (12), 1447–1467. doi:10.1080/08941920.2020.1833617.

Madani, K. (2026) Water Bankruptcy: the formal definition, *Water Resources Management*, **40** (2), 78. doi:10.1007/s11269-025-04484-0.

Mekonnen, M. M. & Hoekstra, A. Y. (2011) The green, blue and grey water footprint of crops and derived crop products, *Hydrology and Earth System Sciences*, **15** (5), 1577–1600. doi:10.5194/hess-15-1577-2011.

Mohanty, B. P., Cosh, M. H., Lakshmi, V. & Montzka, C. (2017) Soil moisture remote sensing: state-of-the-science, *Vadose Zone Journal*, **16** (1), 1–9. doi:10.2136/vzj2016.10.0105.

Molden, D. (1997) *Accounting for Water use and Productivity, SWIM Paper 1*. Colombo, Sri Lanka: International Water Management Institute.

Morbidelli, R., Saltalippi, C., Flammini, A. & Govindaraju, R. S. (2018) Role of slope on infiltration: a review, *Journal of Hydrology*, **557**, 878–886. doi:10.1016/j.jhydrol.2018.01.019.

Mourad, R., Schoups, G., Bastiaanssen, W. & Kumar, D. N. (2024a) Expert-based prior uncertainty analysis of gridded water balance components: application to the irrigated Hindon River Basin, India, *Journal of Hydrology: Regional Studies*, **55**, 101935. doi:10.1016/j.ejrh.2024.101935.

Downloaded from iwaponline.com/jwcc/article-pdf/17/9/2484/1638061/jwc2026225.pdf
by Delft University of Technology user

Mourad, R., Schoups, G. & Bastiaanssen, W. (2024b) A grid-based data-driven ensemble probabilistic data fusion: a water balance closure approach applied to the irrigated Hindon River Basin, India, *European Geosciences Union General Assembly*, **2024** (EGU24), 2267.

Mourad, R., Schoups, G., Rajendran, V. & Bastiaanssen, W. (2026) Joint calibration of multi-scale hydrological data sets using probabilistic water balance data fusion: methodology and application to the irrigated Hindon River Basin, India, *Hydrology and Earth System Sciences*, **30** (3), 525–551. doi:10.5194/hess-30-525-2026.

Nair, A. S., Soman, M. K., Girish, P., Karmakar, S. & Indu, J. (2022) Evaluating SWOT water level information using a large scale hydrology simulator: a case study over India, *Advances in Space Research*, **70** (5), 1362–1374. doi:10.1016/j.asr.2022.05.001.

Neitsch, S. L., Arnold, J. G., Kiniry, J. R. & Williams, J. R. (2009) 1.1 overview of soil and water assessment tool (SWAT) model, *Tier B*, **8**, 3–23.

Niazi, H., Wild, T. B., Turner, S. W., Graham, N. T., Hejazi, M., Msangi, S., Kim, S., Lamontagne, J. R. & Zhao, M. (2024) Global peak water limit of future groundwater withdrawals, *Nature Sustainability*, **7** (4), 413–422. doi:10.1038/s41893-024-01306-w.

Oki, T. & Kanae, S. (2006) Global hydrological cycles and world water resources, *science*, **313** (5790), 1068–1072. doi:10.1126/science.1128845.

Perry, C. (2011) Accounting for water use: terminology and implications for saving water and increasing production, *Agricultural Water Management*, **98** (12), 1840–1846. doi:10.1016/j.agwat.2010.10.002.

Perry, C. (2019) Learning from Water Footprints who loses, who wins, and who caresPage 70 – Policy Quarterly – Volume 15, Issue 3 – August 2019: 70–74.

Pingping, H., Xue, S., Li, P. & Zhanbin, L. (2013) Effect of vegetation cover types on soil infiltration under simulating rainfall, *Nature Environment and Pollution Technology*, **12** (2), 193.

Rodrigues, J. R., Solander, K. C., Cropper, S., Newman, B. D., Collins, A. D., Warren, J. M., Negron-Juarez, R., Gimenez, B. O., Spanner, G. C., Menezes, V. D. S. & Ríos-Villamizar, E. A. (2024) Soil water percolation and nutrient fluxes as a function of topographical, seasonal and soil texture variation in Central Amazonia, Brazil, *Hydrological Processes*, **38** (4), e15148. doi:10.1002/hyp.15148.

Rohde, M. M., Albano, C. M., Huggins, X., Klausmeyer, K. R., Morton, C., Sharman, A., Zaveri, E., Saito, L., Freed, Z., Howard, J. K. & Job, N. (2024) Groundwater-dependent ecosystem map exposes global dryland protection needs, *Nature*, **632** (8023), 101–107. doi:10.1038/s41586-024-07702-8.

Schaake, J. C., Koren, V. I., Duan, Q. Y., Mitchell, K. & Chen, F. (1996) Simple water balance model for estimating runoff at different spatial and temporal scales, *Journal of Geophysical Research: Atmospheres*, **101** (D3), 7461–7475. doi:10.1029/95JD02892.

Schoups, G. & Nasseri, M. (2021) GRACEfully closing the water balance: a data-driven probabilistic approach applied to river basins in Iran, *Water Resources Research*, **57** (6), e2020WR029071. doi:10.1029/2020WR029071.

Sharaf, M. A. M. (2011) Geological and geophysical exploration of the groundwater aquifers of As Suqah area, Makkah district, Western Arabian Shield, Saudi Arabia, *Arabian Journal of Geosciences*, **4** (5), 993–1004. doi:10.1007/s12517-010-0187-1.

Siebert, S., Burke, J., Faures, J. M., Frenken, K., Hoogeveen, J., Döll, P. & Portmann, F. T. (2010) Groundwater use for irrigation–a global inventory, *Hydrology and Earth System Sciences*, **14** (10), 1863–1880. doi:10.5194/hess-14-1863-2010.

Simons, G. W. H., Bastiaanssen, W. G. M., Cheema, M. J. M., Ahmad, B. & Immerzeel, W. W. (2020) A novel method to quantify consumed fractions and non-consumptive use of irrigation water: application to the Indus Basin Irrigation System of Pakistan, *Agricultural Water Management*, **236**, 106174. doi:10.1016/j.agwat.2020.106174.

Smakhtin, V. U. (2001) Estimating continuous monthly baseflow time series and their possible applications in the context of the ecological reserve, *Water Sa*, **27** (2), 213–217.

Sriwongsitanon, N., Suwawong, T., Thianpopirug, S., Williams, J., Jia, L. & Bastiaanssen, W. (2020) Validation of seven global remotely sensed ET products across Thailand using water balance measurements and land use classifications, *Journal of Hydrology: Regional Studies*, **30**, 100709. doi:10.1016/j.ejrh.2020.100709.

Stigter, T. Y., Miller, J., Chen, J. & Re, V. (2023) Groundwater and climate change: threats and opportunities, *Hydrogeology Journal*, **31** (1), 7–10. doi:10.1007/s10040-022-02554-w.

Tapley, B. D., Bettadpur, S., Ries, J. C., Thompson, P. F. & Watkins, M. M. (2004) GRACE measurements of mass variability in the earth system, *Science*, **305** (5683), 503–505. doi:10.1126/science.1099192.

Trambauer, P., Dutra, E., Maskey, S., Werner, M., Pappenberger, F., Van Beek, L. P. H. & Uhlenbrook, S. (2014) Comparison of different evaporation estimates over the African continent, *Hydrology and Earth System Sciences*, **18** (1), 193–212. doi:10.5194/hess-18-193-2014.

Turc, L. (1954) Le bilan d'eau des sols: relations entre les précipitations, l'évaporation et l'écoulement, *Journées de L'hydraulique*, **3** (1), 36–44.

Van Ham, D., Hoekstra, A. Y., Wada, Y., Bouraoui, F., de Roo, A., Mekonnen, M. M., van de Bund, W. J., Batelaan, O., Pavelic, P., Bastiaanssen, W. G. M., Kummu, M., Rockström, J., Liu, J., Bisselink, B., Ronco, P., Pistocchi, A. & Bidoglio, G. (2018) Physical water scarcity metrics for monitoring progress towards SDG target 6.4: an evaluation of indicator 6.4.2 'Level of water stress', *Science of the Total Environment*, **613–614** (2018), 218–232. doi:10.1016/j.scitotenv.2017.09.056.

Vinukollu, R. K., Wood, E. F., Ferguson, C. R. & Fisher, J. B. (2011) Global estimates of evapotranspiration for climate studies using multi-sensor remote sensing data: evaluation of three process-based approaches, *Remote Sensing of Environment*, **115** (3), 801–823. doi:10.1016/j.rse.2010.11.006.

Downloaded from iwaponline.com/jwcc/article-pdf/17/9/2484/1638061/jwc2026225.pdf
by Delft University of Technology user

Vishwakarma, B. D., Devaraju, B. & Sneeuw, N. (2018) What is the spatial resolution of GRACE satellite products for hydrology?, *Remote Sensing*, **10** (6), 852. doi:10.3390/rs10060852.

Von Hoyningen-Hüne, J. (1983) Die interzeption des Niederschlages in landwirtschaftlichen Pflanzenbeständen.

Wada, Y., Van Beek, L. P., Van Kempen, C. M., Reckman, J. W., Vasak, S. & Bierkens, M. F. (2010) Global depletion of groundwater resources, *Geophysical Research Letters*, **37** (20), L20402. doi:10.1029/2010GL044571.

Wada, Y., Wisser, D. & Bierkens, M. F. (2014) Global modeling of withdrawal, allocation and consumptive use of surface water and groundwater resources, *Earth System Dynamics*, **5** (1), 15–40. doi:10.5194/esd-5-15-2014.

Yang, H., Yang, D., Lei, Z. & Sun, F. (2008) New analytical derivation of the mean annual water-energy balance equation, *Water Resources Research*, **44** (3), W03410. doi:10.1029/2007WR006135.

Zeng, Q., Wang, Y., Chen, L., Wang, Z., Zhu, H. & Li, B. (2018) Inter-comparison and evaluation of remote sensing precipitation products over China from 2005 to 2013, *Remote Sensing*, **10** (2), 168. doi:10.3390/rs10020168.

Zhang, L., Hickel, K., Dawes, W., Chiew, F. H., Western, A. W. & Briggs, P. R. (2004) A rational function approach for estimating mean annual evapotranspiration, *Water Resources Research*, **40** (2), W02502. doi:10.1029/2003WR002710.

First received 15 January 2026; accepted in revised form 3 July 2026. Available online 6 August 2026

Downloaded from iwaponline.com/jwcc/article-pdf/17/9/2484/1638061/jwc2026225.pdf
by Delft University of Technology user